3.10 Solar Induced Chlorophyll Fluorescence: Origins, Relation to Photosynthesis and Retrieval

C Frankenberg, California Institute of Technology, Division of Geological and Planetary Sciences, Pasadena, USA; and Jet Propulsion Laboratory, California Institute of Technology, Pasadena, USA
J Berry, Department of Global Ecology, Carnegie Institution for Science, Stanford, CA

© 2018 Elsevier Inc. All rights reserved.

3.10.1	**Introduction**	**143**
3.10.2	**Origins of SIF**	**144**
3.10.2.1	Quenching Mechanisms of Excited Chlorophyll	144
3.10.2.1.1	Summary	147
3.10.2.2	SIF at the Canopy Scale	147
3.10.3	**Global SIF Observations**	**148**
3.10.4	**SIF Retrievals**	**149**
3.10.4.1	Basic Principles of SIF	150
3.10.5	**Additional Challenges from Space**	**156**
3.10.5.1	Notes on Quality Control	158
3.10.6	**Conclusions and Outlook**	**159**
Acknowledgments		**159**
References		**159**

3.10.1 Introduction

Photosynthesis has been key to Earth's habitability, especially since the evolution of oxygenic photosynthesis with the accompanying rise in atmospheric O_2 starting in the Proterozoic era, around 2.5 billion years ago. The conversion of light to chemical energy enables higher life forms and the presence of reduced carbon stocks and molecular O_2 (accumulated products of photosynthesis) provided the fossil fuels for the initiation of our industrialized society. As a visible indicator of photosynthesis, fluorescence emanating from chlorophyll molecules attracted interest more than 100 years ago. In 1874, red fluorescence from a green living leaf was observed to be weaker than from a dilute chlorophyll solution (Müller, 1874), indicating an alternate fate for energy absorbed by chlorophyll in vivo. More quantitative studies of chlorophyll a fluorescence go back to observations by Hans Kautsky and A. Hirsch in 1931 at the Chemical Institute at the University of Heidelberg, Germany (Kautsky, 1931). They discovered the so-called Kautsky effect, a decrease in Chl fluorescence following illumination of dark-adapted leaves. Both studies already indicated an important aspect of chlorophyll fluorescence, namely, that its yield can vary. This effect is caused by variation in the balance of pathways that compete with fluorescence for quenching of the excited chlorophyll state. The porphyrin ring of the chlorophyll molecule is the center of light absorption and fluorescence. In a dilute chlorophyll solution, where fluorescence is the only route for de-excitation, the fluorescence lifetime (τ_F) is about 6 ns and the fluorescence yield (Φ_F) approaches 1. In vivo, the excited chlorophyll state can be quenched by other processes, most notably photosynthesis itself but also quenching to heat; Φ_F is lower (1%–5%) and the τ_F proportionally shorter. Fluorescence in itself is not a significant route for de-excitation of chlorophyll but changes in Φ_F or τ_F can be used to study how absorbed energy is used. On the other hand, when Φ_F is constant, fluorescence can provide information on the total amount of light absorbed, as the amount emitted will be proportional to the total amount of photosynthetically active radiation (PAR) that is absorbed by chlorophyll and associated pigments. **Fig. 1** shows an example of a typical fluorescence spectrum as well as the absorbance spectrum by chlorophyll.

In the following, it will be important to differentiate fluorescence yields (unit-less, representing the fraction of absorbed photons going into fluorescence) from the absolute fluorescence, which is a radiative flux and may indicate changes in yield or the absorbed light flux. This article aims to emphasize the main aspects of how solar-induced chlorophyll fluorescence (SIF) can be used to probe the photosynthetic apparatus and CO_2 exchange of landscapes using remote sensing techniques. Many studies in the past decades made use of fluorescence in various ways (Krause and Weis, 1984, 1991; Flexas et al., 2002; Freedman et al., 2002; Zarco-Tejada et al., 2003; Moya et al., 2004; Rascher et al., 2009; Buschmann, 2007; Lichtenthaler and Rinderle, 1988). We also want to draw attention to several excellent reviews on the history and applications of Chl a fluorescence that have been written, e.g., Lichtenthaler et al. (1986), Papageorgiou et al. (2007), Govindjee (2012), Maxwell and Johnson (2000), Baker (2008). Specifically Porcar-Castell et al. (2014) is most related to the aspects discussed in this article and discusses SIF detail.

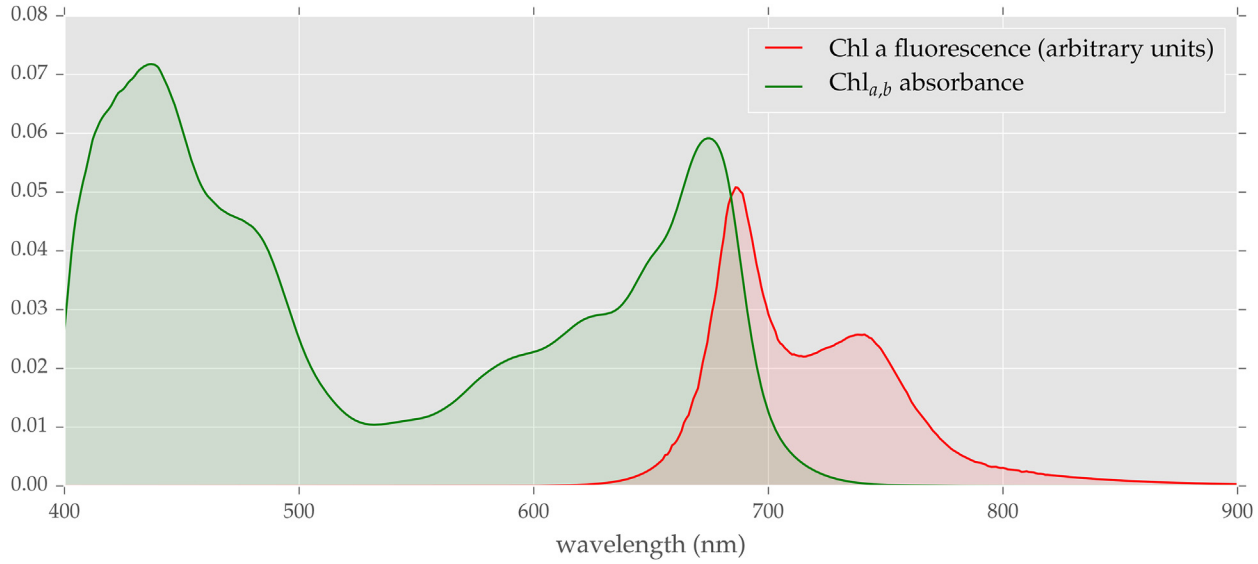

Fig. 1 This graph depicts the absorbance of chlorophyll (both a and b) as well as a typical fluorescence spectrum in arbitrary units. The minimum in the absorbance around 550 nm gives rise to the green color of plants. Around 680 nm, there is an area of overlap, where SIF is increasing and chlorophyll absorption decreasing (a reason for the red edge in vegetation). Thus, the SIF wavelength range up to 700–720 nm is heavily affected by chlorophyll reabsorption, reducing the red peak at 685 nm (Gitelson et al., 1999).

3.10.2 Origins of SIF

3.10.2.1 Quenching Mechanisms of Excited Chlorophyll

Some of the solar photons absorbed by the pigment systems of plant leaves are reemitted as fluorescent photons. In later sections, we will learn how this signal, which constitutes only a very small additive offset (typically $<1\%$–2%) to the overall reflected sunlight, can be obtained using remote sensing techniques.

In the first steps of photosynthesis, captured energy migrates through the antenna system, consisting of chlorophyll molecules and carotenoids bound to proteins. Higher excited states of chlorophyll a (e.g., through absorption of blue light) typically decay rapidly to the more stable, lowest excited state, (Blankenship, 2013). The disposition of energy trapped in this state is under active metabolic regulation that serves to maintain a balance between ultrafast and highly energetic reactions at this stage with the biochemical reactions that fix CO_2 and consume the products of photochemistry. These fast and slow reactions have very different kinetic properties even responding to different environmental variables, but they must mesh seamlessly (Woodrow and Berry, 1988). Two types of photosynthetic units, referred to as PSI and PSII, participate in plant photosynthesis. PSI exhibits a low level of fluorescence ($<30\%$ of PSII), and its fluorescence does not appear to vary with regulation. We will focus our discussion here on PSII, but we note that the fluoresce emission spectrum of PSI differs from PSII; thus its relative contribution to SIF may differ with the wavelength of measurement. The largest contribution of PSI appears to be near 720 nm, but there is a significant contribution from PSI to the 680 nm peak—contrary to previous expectations (Iermak et al., 2016). Considerable variation in the relative height of the 680 and 740 peaks is observed in nature. As shown in **Fig. 1** there is overlap between the absorption and emission spectra of chlorophyll in the region of the 680 nm peak. Variation in chlorophyll content and internal scattering within the leaf or canopy modify the spectrum of fluorescence escaping from leaves or canopies (Gitelson et al., 1999).

The regulation of PSII photochemistry and fluorescence is currently a very active area of research. The apparent objective of this regulation is to minimize the rate of a process termed photoinhibition that occurs by a side reaction of the excited state (for a review, see Zaks et al. (2012).

Our understanding of these regulatory processes is largely derived from laboratory studies using pulse amplitude-modulated (PAM) fluorometry (Schreiber et al., 1986). This instrument resolves the fluorescence elicited by small modulated source of light in the presence of any level of unmodulated light. If the intensity of the modulated light is held constant, then the PAM signal is proportional to the yield of fluorescence Φ_F under the illuminations conditions provided by the unmodulated light source. PAM measurements (a yield) can be related to SIF (a radiance) by the formula $\text{SIF} = \Phi_F \times a\text{PAR}$ where aPAR is the flux of absorbed PAR, keeping in mind that Φ_F measured with a PAM is a relative yield. By active manipulation of the illumination of a leaf, PAM may be used to obtain the yield of photochemistry, Φ_P, and infer the values of rate constants that regulate the disposition of trapped energy during steady-state photosynthesis (Genty et al., 1989; Maxwell and Johnson, 2000; Tol et al., 2014). To understand this, some discussion of theory is necessary.

Under passive illumination, a fraction of absorption events are consumed when the excited state reaches the reaction centers where photochemistry occurs (with fraction Φ_P). This pathway competes with other quenching mechanisms including non-radiative decay (Φ_D), and a regulated process known as nonphotochemical quenching that diverts unneeded energy to heat

(with fraction Φ_N), and, finally, fluorescence (Φ_F)—that is, the escape of a photon when the excited electronic state of a molecule decays to its ground state. To conserve energy, the sum of the above fractions, or quantum yields, must be unity: $\Phi_P+\Phi_N+\Phi_D+\Phi_F=1$, and the partitioning between these is related to corresponding rate constants by

$$\Phi_F = \frac{K_F}{K_P + K_N + K_D + K_F}. \quad (1)$$

The rate constant for decay of the excited state by fluorescence (K_F) and the cross-section for absorption are intrinsic properties of the chlorophyll molecule and this provides an universal yardstick for monitoring the processing of photon energy in photosynthetic membranes. For example, the measured Φ_F in vivo is very low ($\approx 1\%$), so we may infer the sum of the other terms ($K_P+K_N+K_D$) is about $100 \times K_F$. Two of these rate constants, K_P and K_N, are variable, while K_F and K_D remain constant. K_P may decrease when reaction centers accumulate in a reversible, inactive state, when electrons produced in photochemistry accumulate at the reaction centers. K_N generally increases when conditions cause K_P decreases. Nonphotochemical quenching is regulated by molecular switches within the reaction center complexes (Schlau-Cohen, 2015) that influence the probability of an excited state being used for photochemistry or being dissipated to heat. These switches are controlled by factors such as the pH of the environment of the reaction center and the availability of certain xanthophyll pigments (Niyogi and Truong, 2013), and these pigment changes may quantified by the photochemical reflectance index (PRI) (see chapter by Hilker in this volume).

The rate of photochemistry can be expressed by an analogous equation:

$$\Phi_P = \frac{K_F}{K_P + K_N + K_D + K_F}. \quad (2)$$

The behavior of this system differs depending upon whether the flux of absorbed PAR is rate-limiting or rate-saturating for the overall photosynthetic process (see **Fig. 2**). When light is limiting, it is to the plants' advantage to maximize Φ_P. To accomplish this, K_N should be minimized and K_P maximized. Measurements of the quantum requirement for O_2 evolution (after accounting for differences in absorptance) are quite constant among species except when PSII units become damaged by photoinhibition (Demmig and Björkman, 1987). On the other hand, when light becomes rate-saturating, the rate of photochemistry is constrained by other reactions and Φ_P must vary in response to changes in light intensity. Inspection of Eq. 2 indicates that this objective could be met simply by reducing K_P. However, we know from PAM fluorometry that K_N increases with a corresponding recovery of K_P. As shown in **Fig. 2** these changes are typically such that $\Phi_P+\Phi_N$ and Φ_F are about constant. However, application of an inhibitor that blocks development of K_N strongly stimulates Φ_F, while having no effect on Φ_P (Schäfer and Björkman, 1989). This illustrates a key feature of this regulatory system, that there is no exact coupling between Φ_F and Φ_P. This coupling depends upon plant specific regulation of K_N.

Van der Tol and coworkers (Tol et al., 2014) developed an approach to parameterize the behavior of K_N as a function of the strength of the feedback on photochemistry from the dark reactions. They found that the feedback was stronger for leaves that had previously experienced drought than leaves that had not. **Fig. 3** shows simulated responses based on a parameterization with leaves undergoing or recovering from drought stress. The simulations illustrate the effect of different levels of the CO_2-fixing enzyme Rubisco (V_{cmax}) in response to the absorbed quantum flux of PAR. Shown are the fluorescence yield (Φ_F), the

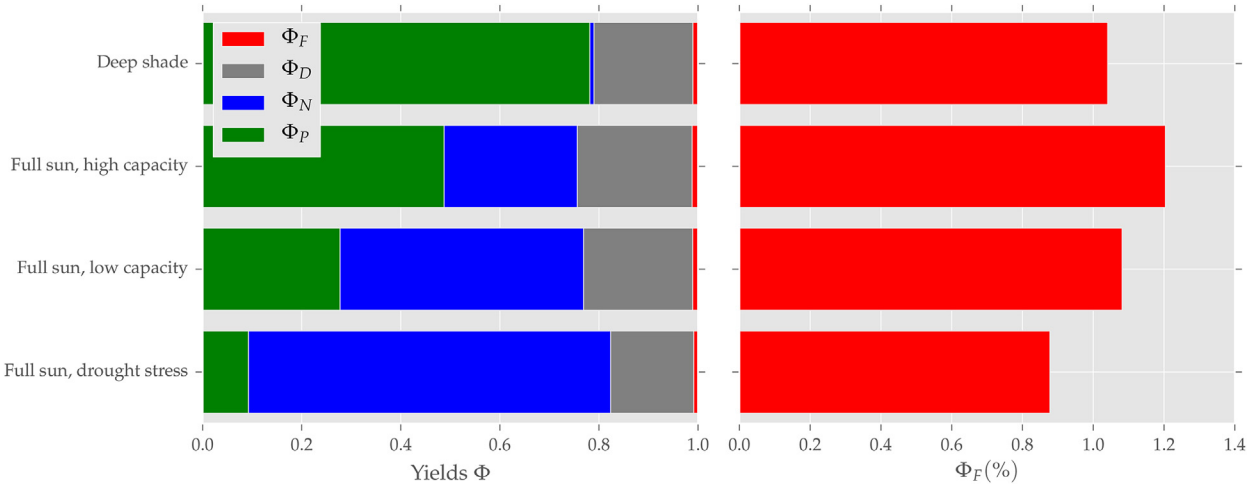

Fig. 2 Quantum yields (Φ) for the four pathways used by leaves to process photons depend on whether the leaf is shaded or exposed to full sun, whether the leaf has a high or low photosynthetic capacity, and whether drought stress is present. In the histogram, *green* denotes photosynthesis (PSII yield); *blue*, nonphotochemical quenching; *gray*, nonradiative decay; and *red*, fluorescence. The results shown here were obtained with a laboratory instrument called a PAM fluorometer. As the *right panel* shows, the fluorescence quantum yield changes less than the PSII yield but also noticeably with varying conditions, especially once nonphotochemical quenching becomes dominant.

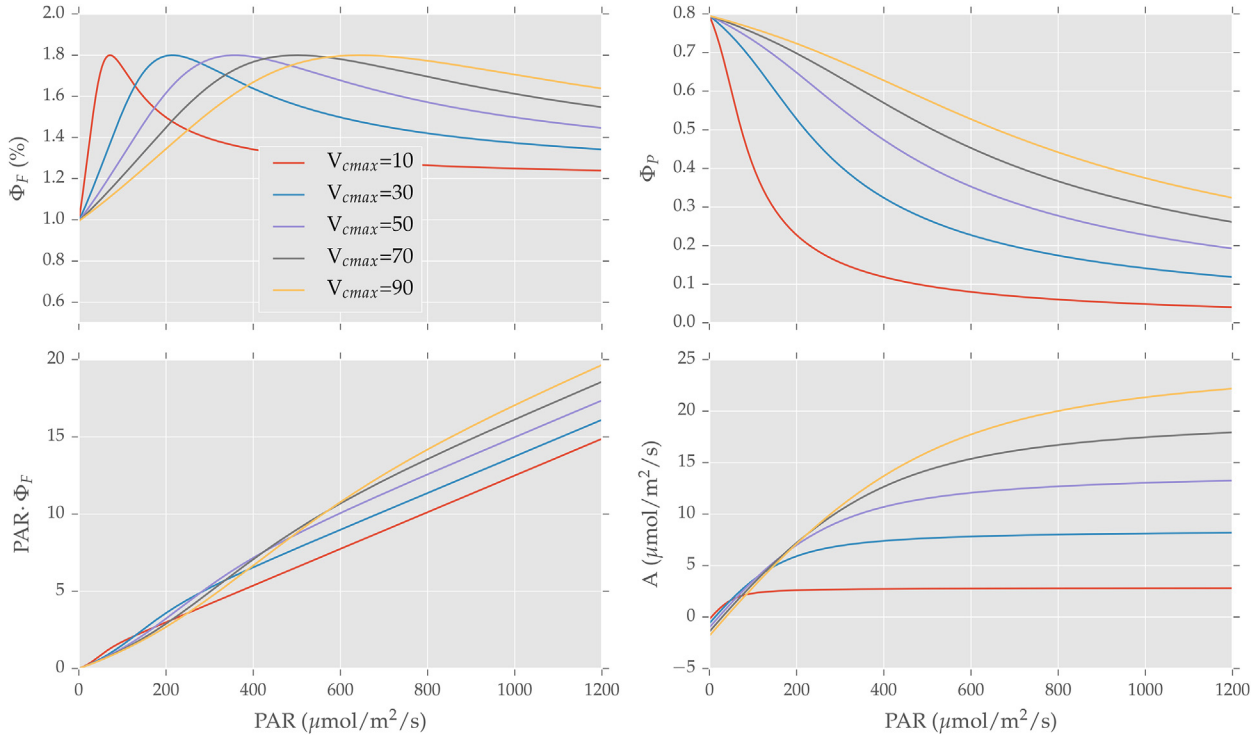

Fig. 3 Simulated response of photosynthetic CO_2 assimilation (A), photochemical yield, (Φ_P), fluorescence yield, (Φ_F), and fluorescence radiance (PAR $\times$ Φ_F) to variation in the absorbed flux of PAR and with variation in the activity of the activity of the CO_2-fixing enzyme, Rubisco (V_{cmax}). Decreasing the V_{cmax} progressively increases the feedback from the dark reactions on the processing of absorbed photons. Φ_F declines with increasing PAR above the point of light saturation due to increasing nonphotochemical quenching associated with this feedback. These simulations were conducted with the TB-12 module of SCOPE (version 1.60), with the parameterization of Φ_F vs. Φ_P (Tol et al., 2014). Note that the parameterization can vary with vegetation type and prehistory.

photochemical yield (Φ_P), the fluorescence radiance (PAR $\times$ Φ_F), and the rate of CO_2 assimilation. Decreasing V_{cmax} causes the rate-saturated rate of photosynthesis to decrease and the transition from the light-limiting to the light-saturating condition to occur at a lower PAR. This imposes a ceiling on the rate of photochemistry and Φ_P must decline when the ceiling is reached. Φ_F exhibits complex behavior, first increasing and then declining with increasing PAR as nonphotochemical quenching kicks in. The fluorescence radiance (expected SIF) increases at first nonlinearly and then linearly with PAR. At high levels of PAR—as might occur during a midday satellite overpass, the level of SIF is higher for leaves with high than low V_{cmax}. It is important to note that this is an illustration of the general pattern observed with leaves—the exact responses may differ. The two parameterizations given in Tol et al. (2014) span the likely range of plants in nature - except for evergreen conifers exposed to winter contitions (Porcar-Castell et al., 2014).

It is often surprising to researchers who have some familiarity with fluorescence that the variations in SIF yields are small. The key to understanding this behavior is the photoinhibition reaction referred to earlier. As shown in **Fig. 2**, physiological regulation of Φ_N is such that the sum $\Phi_P + \Phi_N$ remains about constant as environmental or physiological conditions change. If this were not the case, the fraction of excitation going to photodamage (and fluorescence) would increase. Photoinhibition has been characterized as a photon counter (Park et al., 1995). About one in a million photon absorption events results in an aberrant photochemical reaction that damages a protein in the reaction center. When this occurs, the center and its associated pigments become nonfunctional. If it were not for an active repair mechanism, this damage would accumulate and photosynthesis would slowly stop. This repair mechanism requires active protein synthesis and is a significant drain on the energy economy of photosynthesis. It is thought that the rate of photoinhibition is related to the lifetime of the excited state by a first-order rate constant. If so, the longer the excited state "hangs around" the more probable this side reaction—and incidentally fluorescence too. It appears that a regulatory mechanism of plants increases K_N just enough to permit photochemistry go at the rate permitted by downstream reactions (light-independent or so-called "dark" reactions), while avoiding a backup in quenching of excited states, thus minimizing (but not eliminating) the rate of photoinhibition. These same regulatory processes tend to keep Φ_F low and stable. Indeed, it has been shown that application of chemicals that blocks nonphotochemical quenching (the increase in K_N) stimulates the rate of photoinhibition (Schäfer and Björkman, 1989). One effect of nonphotochemical quenching is to speed consumption of the excited state; the obvious result is to keep fluorescence yield low. However, the associated impact on photoinhibition may be of greater significance for natural selection, and this hypothesis provides a rationale to explain the observed behavior of fluorescence.

3.10.2.1.1 Summary

The yield of fluorescence emitted by the PSII complexes is directly proportional to the average lifetime of excited states in the pigment systems. Under ideal conditions most of the captured excited states are used for photochemistry, but when the flux of absorbed photons is in excess of that needed to support CO_2 fixation, photochemical reaction centers must close and the lifetime of excited states could increase with a corresponding increase in a side reaction leading to photoinhibition. To avoid this fate, plants increase the activity of non-photochemical quenching mechanisms that dissipate excited states as heat. This competes with photochemistry, shortening the life time of excited states, minimizing the rate of photoinhibition and stabilizing the fluorescence yield - while also permitting photosynthesis to proceed at near its maximum possible rate. These regulatory mechanisms (stomata for light?) tend to keep the yield of SIF low and relatively constant with a tendency to decrease when non-photochemical quenching is strong. As shown in Fig. 3, there is a nearly proportional relation between SIF and GPP when light is limiting for photosynthesis but this diminishes when photosynthesis becomes light-saturated.

3.10.2.2 SIF at the Canopy Scale

Pioneering work of Yang et al. (2015) at the Harvard Forest flux site provides the first long-term and continuous observations of SIF and GPP from ground based observations. These studies confirm correlations between SIF and GPP that have been obtained from analysis of satellite measurements averaged and aggregated to monthly time steps on a half degree grid. Here we seek to rationalize this strong correlation with what we have learned of the physiology. Additional biophysical processes come into play when we consider fluorescence measured above a canopy. It is useful to represent this in the form of a simple equation:

$$\mathrm{SIF} = \mathrm{PAR} \cdot f\,\mathrm{PAR} \cdot \Phi_F \cdot \Omega_C \tag{3}$$

where PAR is the incident flux of photosynthetically active radiation, f PAR is the fraction of PAR absorbed by photosynthetic pigments, Φ_F is the yield of fluorescence in the wavelength band of the measurement, and Ω_C is the probability that an emitted photon will escape the canopy to be detected. Evaluation of the terms of this equation can be very challenging for a complex canopy, especially as yields and escape probability will vary with leaf display and depth in a canopy. The following sections provide a qualitative discussion of these terms. A more quantitative understanding can be obtained from the SCOPE model, an integrated model of soil–canopy spectral radiances, photosynthesis, fluorescence, temperature, and energy balance (Tol et al., 2009, 2014; Vilfan et al., 2016, and associated papers).

It is interesting that we can write a parallel equation to Eq. 3 for the rate of gross primary photosynthesis (expressed as CO_2 fixation),

$$\mathrm{GPP} = \mathrm{PAR} \times f\mathrm{PAR} \times \mathrm{LUE}, \tag{4}$$

where LUE is the apparent light-use-efficiency (mol CO_2/mol PAR). If we eliminate PAR × f PAR and combine the equations, we obtain

$$\mathrm{GPP} = \mathrm{SIF} \times \frac{\mathrm{LUE}}{\Phi_F \times \Omega_C}. \tag{5}$$

This indicates that GPP could be proportional to SIF (as has been observed, see below). One interpretation is that physiological control of SIF is a good proxy for LUE. Another is that SIF is a good proxy for the flux of absorbed PAR. This is still an area of active research. However, we note that the flux of PAR absorbed by the photosynthetic pigments of the canopy is usually an uncertain quantity. While it is simple to measure or model the absorbed PAR of a canopy, it is much harder to compute the fraction that is absorbed by the photosynthetic pigments. Zhang et al. (2005) made a compelling argument that traditional estimates of fPAR based on vegetation indices can under- or overestimate the fraction of PAR absorbed by the chlorophyll of the vegetation by a variable extent. They reviewed several methods that have been developed to improve this, but it has been difficult to validate these methods as it is quite difficult to directly estimate the flux of PAR absorbed by chlorophyll. However, plausible estimates of fPAR(chl) are more strongly correlated with GPP at several flux sites than the conventional fPAR products. It is useful to note the potential that SIF could be used to test and improve the understanding of this key parameter.

A number of studies have begun to address the question of what controls the level of SIF escaping from a canopy. Zhang et al. (2014) showed that an observed correlation of SIF with GPP measured at several flux sites could be explained by positing a relationship between SIF and the V_{cmax} of Rubisco. On the other hand, Verrelst et al. (2015) and Koffi et al. (2015) concluded from model sensitivity studies with SCOPE that SIF is most sensitive to canopy properties such as chlorophyll content, leaf area index (LAI), and leaf angle distribution, with lesser sensitivity to Rubisco V_{cmax}. Recently van der Tol et al. (2016) conducted a study using observed measurements of SIF and reflectance from crop canopies to fit parameters of the SCOPE (*Soil Canopy Observation, Photochemistry and Energy Fluxes*) model. Interestingly, when the model was fit to the observed reflectance properties, no additional fitting was needed to fit the observed SIF. Simulations that included control of Φ_F by V_{cmax} fit marginally better than simulations where Φ_F was fixed. This empirical study supports the argument that SIF is primarily determined by the canopy structure—presumably through the fPAR relationship—not by canopy biochemistry. This seems to contradict the work of Zhang et al. (2014) and coworkers that attribute variation in SIF to V_{cmax}. However, recent work by Badgley et al. (2017) may help to resolve these conflicting views. They find that SIF and a new a new structural parameter, NIRv, correlate better with canopy GPP than does fPAR. In other words, variation in fPAR is not sufficient to explain variation in SIF or GPP, but SIF is also related to canopy structure. Canopies with similar fPAR (e.g., crop

or evergreen needle leaf canopies) can apparently emit different levels of SIF and have different levels of GPP. They suggest that this could be due to differences in the fraction of sun and shade leaves making up the canopies. More SIF and a higher near-infrared reflectance (NIRv) corresponds to a larger fraction of sun leaves, and it follows that sun leaves would have a higher V_{cmax} than shade leaves. This interpretation is supported by analysis of the available data on GPP at flux sites. If correct, this hypothesis would indicate that the correlation between SIF and V_{cmax} observed by Zhang et al. (2014) is rooted in the canopy structure and that there is a correlation of structure with photosynthetic capacity and V_{cmax}. More work is needed to examine this possibility, but studies in this field are rapidly progressing (Rossini et al., 2016; Migliavacca et al., 2017).

3.10.3 Global SIF Observations

The first space-based SIF observations have been performed by Guanter et al. (2007), using the medium-resolution imaging spectrometer on board the ENVIronmental SATellite (ENVISAT) using narrow band observations in the oxygen A-band in a small regional domain. The need to have constant atmospheric conditions and the use of nonfluorescing reference targets restricted the spatial domain of the analysis. The first truly global SIF measurements were obtained using high-resolution spectra acquired by the Japanese GOSAT mission launched in 2009 (Joiner et al., 2011; Frankenberg et al., 2011b; Guanter et al., 2012). This capability, enabled by the high spectral resolution of the GOSAT Fourier transform spectrometer, spurred wide interest in global SIF studies in the carbon cycle community. These groups found a very strong linear correlation of SIF radiance with current best estimates of GPP. Further studies enabled SIF retrievals from other existing satellites as well, providing a multitude of SIF satellite products from instruments such as the Global Ozone Monitoring Experiment-2 (GOME-2) instruments onboard the Meteorological Operational Satellites MetOp-A, and MetOp-B, SCIAMACHY on ENVISAT, and the Orbiting Carbon Observatory-2 (OCO-2) (Frankenberg et al., 2011a,b; Frankenberg et al., 2012, 2014; Joiner et al., 2011, 2012, 2013, 2016; Guanter et al., 2010a; Köhler et al., 2015; Wolanin et al., 2015). These measurements have already been used in studies of crop productivity (Guanter et al., 2014; Guan et al., 2016), drought impacts (Yoshida et al., 2015; Sun et al., 2015; Parazoo et al., 2015), tropical photosynthesis seasonality (Lee et al., 2013; Guan et al., 2015), or variations at high latitudes (Luus et al., 2017; Jeong et al., 2017).

Fig. 4 shows SIF retrieved from the OCO-2 satellite as a simple example for a typical summer month, with global maxima in the U.S. corn belt. In the future, more measurement with higher spatial resolution will be available, most notably TROPOspheric Monitoring Instrument (TROPOMI) (Guanter et al., 2015). The first dedicated SIF mission will be the FLuorescence EXplorer (FLEX) (Stoll et al., 1999; Rascher et al., 2008; Moreno et al., 2014; Rascher et al., 2015; Drusch et al., 2016), chosen by ESA as Earth Explorer 8 mission to be launched in 2022. Multiple airborne campaigns have already been conducted with a similar instrument (Rascher et al., 2015; Wieneke et al., 2016; Rossini et al., 2015).

Here, we do not attempt to provide a comprehensive overview of available satellite, airborne or ground-based measurements but rather focus on a few common retrieval principles. As illustrated before, more work has to be done to understand why SIF and GPP correlate so well empirically even though saturation effects in GPP are expected to be stronger than for SIF. Various studies attempt to tackle these questions (Damm et al., 2010; Campbell et al., 2007; Yang et al., 2015; Zhang et al., 2016; Lee et al., 2015; Verrelst et al., 2015, 2016; Rossini et al., 2015, 2016) and one of the primary challenges is to compute changes in fluorescence yield (stress)

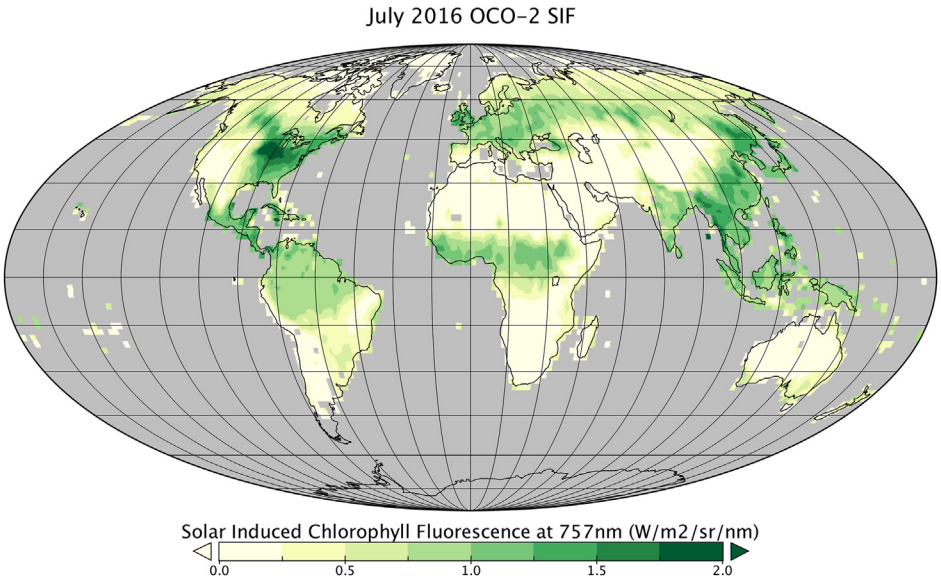

Fig. 4 SIF monthly average from July 2016 using data from the Orbiting Carbon Observatory-2. The corn belt in the United States can be clearly observed as a dominant feature, as was initially reported by Guanter et al. (2007).

from changes in absorbed radiation. At the current temporal and spatial scales, this task is difficult from space as changes in chlorophyll content at weekly time-scales dwarf the impact of the fluorescence yield and dynamic downregulation induced by the xanthophyll cycle and associated changes in K_N. Additional information on the xanthophyll cycle status, which triggers nonphotochemical quenching (and is described in more detail by Thomas Hilker in this book) would be very complementary to SIF and better enable us to compute the stress impact from current observations.

3.10.4 SIF Retrievals

There are various methods that have been developed to infer SIF (or any additional offset for that matter) from spectral measurements. Meroni et al. (2009) and references therein summarize more recent methods and principles of SIF retrieval strategies with a particular focus on the oxygen absorption bands using ground-based and airborne observations. Here, we will focus more on the Fraunhofer lines and the application of full spectral fitting using forward modeling of the recorded radiance. We will also discuss the advantages and disadvantages in using telluric absorption features, especially when using space-borne remote sensing, which has recently been established using high-resolution spectrometers covering parts of spectrum of the SIF emission spectrum (Frankenberg et al., 2011a,b, 2012, 2014; Joiner et al., 2011, 2012, 2013; Guanter et al., 2010a).

In this section, we will discuss the overall effect of solar-induced chlorophyll fluorescence on measurements of reflected light at the canopy scale. Particular focus will be on how to disentangle the SIF contribution from the measured radiances, which are mostly composed of reflected sunlight with SIF adding only a small amount, typically 0.5%–2%. In some ways, this problem is analogous to visually observing mineral fluorescence (e.g., from Fluorspar) in the visible spectrum upon illumination with UV light. In bright daylight, the fluorescence cannot be discerned from the background radiation but in a dark room, with only UV light present, it can be observed with the naked eye. Observing SIF under natural conditions by definition precludes such a setup as solar light encompasses the entire spectral range of SIF. However, there are absorption features within the incoming solar light (so-called Fraunhofer lines) as well as within the Earth's atmosphere (telluric lines). The Fraunhofer lines are spectral lines named after the German physicist Joseph von Fraunhofer. They are caused by elements in the sun's atmosphere, specifically the photosphere and chromosphere, absorbing light at specific wavelength related to the discretized energy levels within the respective element, for example, Na, Mg, Ca, or Fe. While these features are not entirely opaque, they offer darker spectral sections within the observed radiation. These can be used to differentiate the additive offset caused by SIF. Figuratively speaking, they are a dark room (not perfectly black but at least gray) in spectral space. This is the basis for almost all fluorescence retrieval strategies developed so far. To our knowledge, Plascyk and Gabriel (1975) were the first to devise an airborne spectrometer system to employ this technique on a Fraunhofer line at 598 nm, nicely summarizing the underlying principle:

> "[…] a purely reflecting scene, having no luminescence component, will replicate the ratio obtained in pure sunlight of the energy in a narrow band within a selected Fraunhofer zone to the energy in an equal bandwidth in the neighboring continuum; i.e., reflected sunlight is coded. A scene containing fluorescence, however, changes the code by disturbing the ratio."

The principle of the in-filling of Fraunhofer lines to detect an additive signal was already used in astronomy for a long time and goes back to Kozyrev (1956), suggesting that lunar luminescence (for not entirely known reasons) could be detected by comparing the depths of Fraunhofer lines reflected from the Moon with those from direct sunlight. Potter et al. (1984) provide an extensive overview on the history and potential causes for lunar luminescence and cite even earlier initial studies. Interestingly, Grainger and Ring (1962c) were also interested in lunar luminescence measurements using Fraunhofer line in-filling techniques. However, they also detected reductions in the Fraunhofer line absorption depth when looking at scattered sunlight as compared to direct sunlight. This study on *Anomalous Fraunhofer Line Profiles* (Grainger and Ring, 1962a) was later confirmed to be caused by rotational Raman scattering by N_2 and O_2 molecules in the Earth's atmosphere (Brinkmann, 1968; Kattawar et al., 1981), effectively filling in the Fraunhofer lines. This inelastic scattering effect scales with the Rayleigh cross section, thus with λ^{-4}. Especially in the UV and visible spectral ranges, it has a considerable impact on the shapes of Fraunhofer lines. This so-called Ring effect is crucial for atmospheric trace gas retrievals using absorption spectroscopy (Joiner et al., 1995; Chance and Spurr, 1997) as its magnitude is often larger than those caused by optically thin absorbers such as NO_2 or SO_2. The history of Fraunhofer line applications is indeed somewhat convolved: initially, they were intended for lunar luminescence measurements (Grainger and Ring, 1962b; Potter et al., 1984) but led to the detection of the Ring effect (Grainger and Ring, 1962a; Brinkmann, 1968) now widely used in atmospheric sciences (Joiner et al., 1995; Chance and Spurr, 1997; Platt and Stutz, 2008). This may explain why the first truly global maps of SIF derived using only Fraunhofer lines were developed by the atmospheric science community (Joiner et al., 2011; Frankenberg et al., 2011b) using satellites that were intended for measurements of atmospheric trace gases.

The coincidence in measuring SIF is also related to the application of the oxygen A-band, which is being used for accurate retrievals of changes in the atmospheric light-path, which are necessary for retrievals of atmospheric methane and carbon dioxide. The spectral channels used for the oxygen A-band happen to overlap with SIF and include a few Fraunhofer lines as well. Initially, another oxygen band at 1.27 μm was envisioned but discarded due to a stronger air-glow effect (Crisp et al., 1996). This historical

perspective is an excellent example of the classical *your noise is my measurement* problem, which is often encountered when different scientific disciplines work with similar datasets for varying purposes.

We shall not yet fully disregard the rotational Raman scattering impact on SIF measurements, especially at shorter wavelengths. However, Vasilkov et al. (2013) performed a model sensitivity study and showed that the effect is relatively small and only important at very large solar zenith angles (SZAs) and low surface albedos.

3.10.4.1 Basic Principles of SIF

In the absence of atmospheric scattering (purely geometric considerations here), a measured nadir (downward-looking) measurement L^λ over a lambertian surface with wavelength dependent reflectance ρ^λ can be written as

$$L^\lambda = \frac{I_0^\lambda \mu_0 \rho^\lambda T_\downarrow^\lambda T_\uparrow^\lambda}{\pi} + SIF^\lambda T_\uparrow^\lambda, \tag{6}$$

where I_0^λ is the solar irradiance spectrum, μ_0 is the cosine of the SZA, and T^λ is the atmospheric transmission along the lightpath of the photons reaching the detector (which might be right above the canopy or in space), separated by upwelling and downwelling (using arrows). The upper case $^\lambda$ notation indicates quantities that can vary with wavelength.

In the following, we will describe in detail how absorption features can be utilized to discriminate SIF from changes in the background reflectance and how further simplifications to Eq. 6 can be used to solve the inverse problem for SIF^λ given the measurement vector L^λ.

Fig. 5 shows a disk-integrated solar transmission spectrum at native resolution generated using a solar line-list from http://mark4sun.jpl.nasa.gov/toon/solar/solar_spectrum.htm. The term "disk-integrated" relates to the average solar spectrum using the entire solar disk. Due to the rotation of the sun, there is a varying Doppler shift associated with different regions of the sun, which leads to an overall broadening of the solar spectrum if the entire disk is observed. Here, we only consider disk-integrated spectra, which are most applicable under natural conditions. As can be seen, the spectral range depicted in Fig. 5 is full of narrow solar features, originating from absorption in the sun's chromosphere, with transmissions as low as 20%. When observing this solar spectrum, we have to take the spectral resolution of the instrument into account, which smoothes this theoretical transmission spectrum and thereby changes the minima in the transmission spectrum. The spectral resolution is typically provided in full width at half maximum (FWHM). For simplicity, we use a Gaussian instrument line shape in the following considerations (for a Gaussian line-shape, the FWHM is equivalent to $2\sqrt{2ln(2)}\cdot\sigma$, with σ being the standard deviation of the Gaussian distribution).

Fig. 6 shows the solar transmission spectrum at various spectral resolutions, ranging from 0.05 to 0.5 nm. The top panel shows the entire spectral range between 600 and 870 nm, while the lower panel focuses on the range of the far-red fluorescence peak around 740 nm. Even at the high spectral resolution of 0.05 nm, the transmission minima are largely dampened for the narrow solar features, with the exception of a few very broader features at 656 and above 850 nm.

With this solar transmission spectrum, we can easily illustrate the effect of an additive signal such as SIF. For simplicity, let us assume the flat transmission spectrum with a continuum level of 1.0 and a spectrally invariant offset of 1%, i.e., 0.01 in absolute

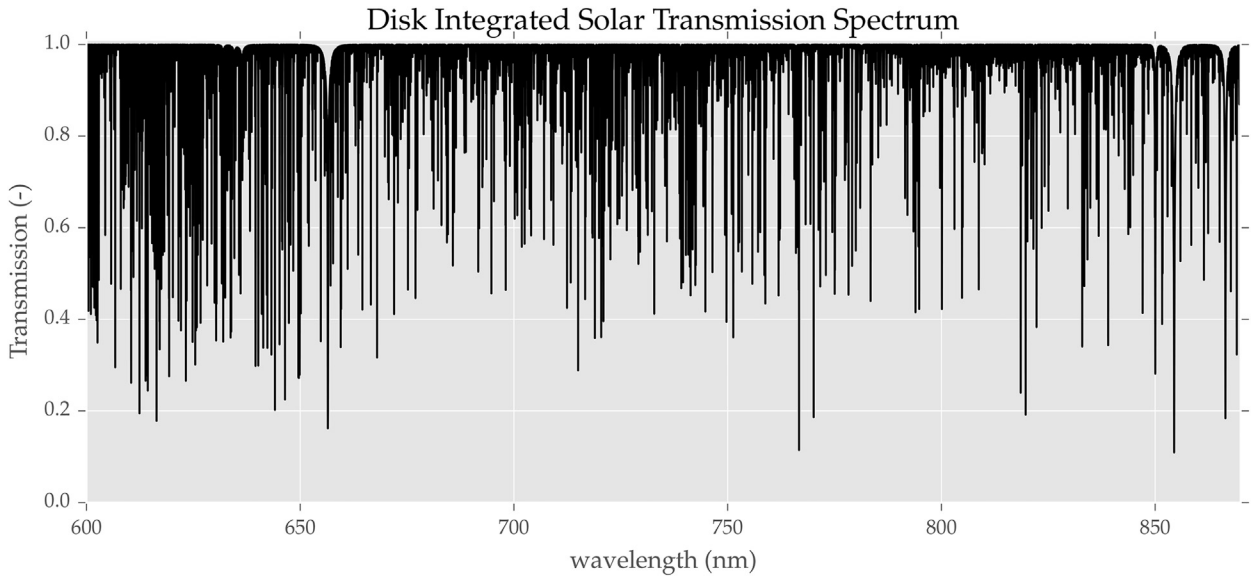

Fig. 5 High-resolution transmission spectrum for a disk integrated solar spectrum. The disk-integrated lines are wider than center-only observations owing to Doppler broadening due to the sun's rotation.

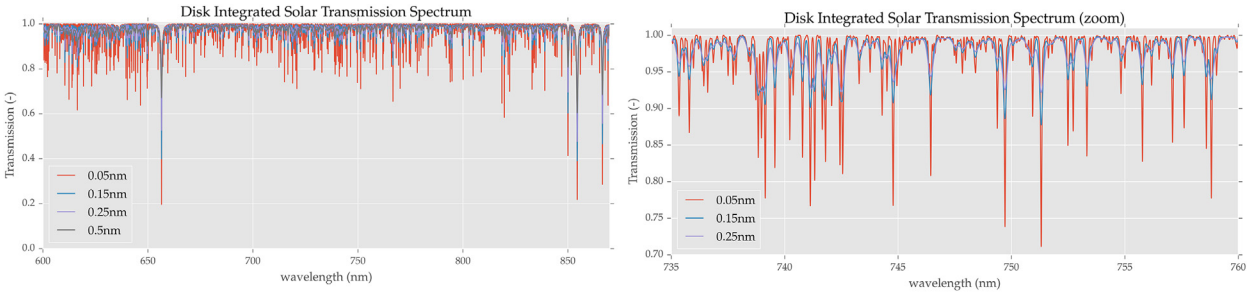

Fig. 6 This graph depicts the solar transmission spectrum at different spectral resolutions in the range of primary interested for solar-induced chlorophyll fluorescence.

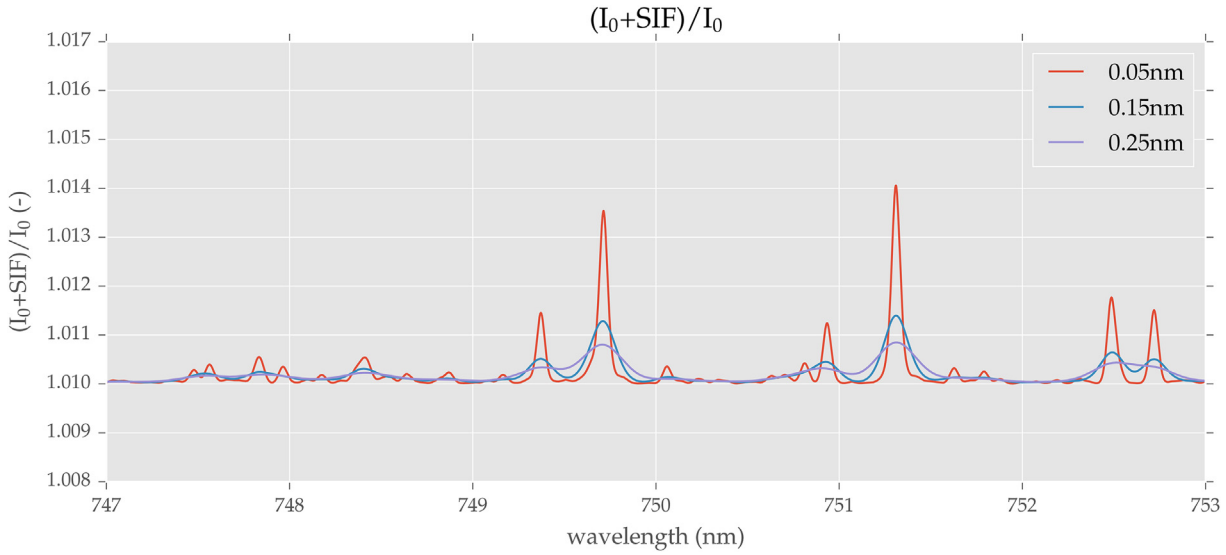

Fig. 7 This graph shows the impact of a spectrally flat additive signal (1% of the original continuum signal) on the depth of Fraunhofer lines. Changes in the depth are immediately obvious in ratio spectra, which would be spectrally flat in the absence of additive signals. In this case, the ratio spectrum changes from around 1 through 4‰, depending on the instrument's spectral resolution.

terms. This additive term will change the fractional depth of each of the absorption lines, dependent on their actual transmission: e.g., a Fraunhofer line with 50% transmission has a fractional depth of 0.5 (0.5/1) before the addition of SIF and (0.5 + SIF)/(1 + SIF) = 0.505 with the additive SIF offset of 1%.

This simple calculation already shows one of the main challenges: a change of 0.005 is 0.5% of the continuum level radiance, requiring a high signal-to-noise ratio (SNR) if we want to actually measure this signal to within 10%; 0.5% corresponds to an SNR of 200 and we would need at least a factor 10 as much if we had just a single Fraunhofer line to discern the signal 1% SIF signal to within 10% relative accuracy.

In the following, we will exemplify the SIF effect on a small spectral range around 750 nm, which includes two relatively strong Fraunhofer lines and is devoid of strong telluric absorptions (see also Khosravi et al. (2015)). **Fig. 7** shows the impact of a 1% additive SIF signal to a ratio spectrum, i.e., the ratio of a transmission with and without an additive SIF signal. It should be noted that any elastic scattering within the atmosphere or reflected light from the surface acts on the spectra in a multiplicative way with no high-frequency spectral variations. In the absence of an additive signal such as SIF, ratio spectra under different atmospheric or surface conditions would thus always be spectrally flat and could be fitted with a simple low-order polynomial in spectral space. In the ratio with SIF, however, we see high-frequency spectral variations due to the larger fractional in-filling within the Fraunhofer lines. The strongest lines show a sharp spectral change with a magnitude of around 4%. As a 1% SIF offset was used, the baseline minimum is 1.01, but it is important to note that we do not need to know the absolute baseline level as we only have to look at the high spectral frequency in-filling, which can be fully decoupled from the baseline changes. This technique is very similar to differential optical absorption spectroscopy (DOAS, Platt and Stutz (2008) and references therein), which disentangles the high-frequency structures induced by gaseous absorption features from broad-band features induced by spectrally variant surface reflectances as well as spectrally smooth atmospheric effects. The measurement requirements and challenges in the atmospheric DOAS community are well documented in the literature (Platt and Stutz, 2008, and reference therein).

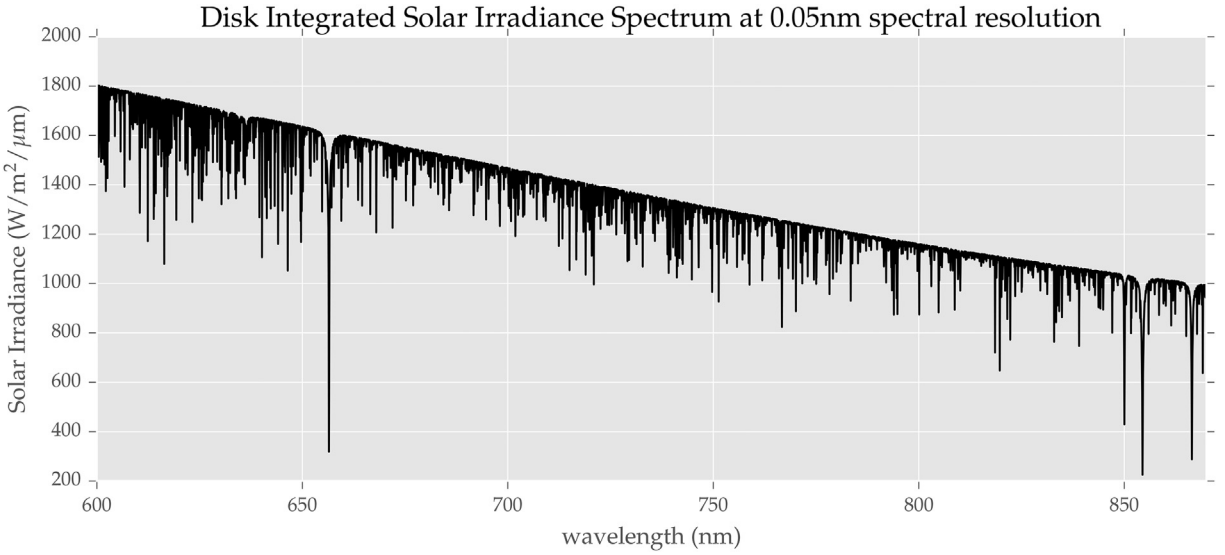

Fig. 8 This graph shows the absolute radiometric solar irradiance spectrum with 0.05 nm FWHM spectral resolution.

If we just focus on a small microwindow of a few nanometers, we do not need to know the spectral shape of SIF a priori. However, the more Fraunhofer lines we can cover, the more precise a retrieval will be. If we expand the spectra range, we have to take other effects into account. Thus, let us now move from the simple example to how SIF would alter the entire spectral range from 650 through 850 nm under more realistic conditions. Toward this goal, we need to model the solar irradiance spectrum, which provides the incoming radiation at the top of atmosphere.

Fig. 8 shows a solar model, constructed using the transmission model as mentioned before (at 0.05 nm FHWM) with a solar continuum derived from data presented in Thuillier et al. (2004). In the absence of inelastic atmospheric scattering (such as rotational Raman scattering), the optical depths of the absorption features that do not overlap with atmospheric absorptions will remain invariant to elastic scattering within the atmosphere as well as from the Earth's surface, i.e., all effects are multiplicative, akin to multiplying the depicted spectrum with a polynomial:

$$L^{\lambda} = I_0^{\lambda} \cdot \sum_{i=0}^{n} a_{i^*} \lambda^i. \tag{7}$$

This equation basically assumes that all surface and atmospheric effects, i.e., $\frac{\mu_0 \rho^{\lambda} T^{\lambda}\downarrow T^{\lambda}\uparrow}{\pi}$ can be approximated with the polynomial $\Sigma_{i=0}^{n} a_{i^*} \lambda^i$, which is valid if spectral variations in $T^{\lambda}\downarrow$, $T^{\lambda}\uparrow$, and ρ^{λ} are smooth and can be fitted with a polynomial term. This is valid as long as the spectral range is devoid of spectrally sharp atmospheric absorption features.

When sharp atmospheric absorption features have to be considered, the use of Eq. 7 becomes invalid as the depths of the absorptions depend on the so-called slant optical density, an integral of the product of gas concentration and absorption coefficient along the light-path of the photons reaching the detector. This would not allow us to model the measured radiance with a simple multiplicative polynomial term. In our view, this invariance with respect to scattering is the biggest advantage of using Fraunhofer lines for SIF retrievals as it is less prone to biases induced by ambiguities that might occur when using atmospheric absorption features (Frankenberg et al., 2011a). These ambiguities might be small when observing SIF directly above the vegetated surface but will increase with the distance between the actual location of SIF emission and the observer.

Fig. 9 illustrates the key components in radiance spectra obtained in down-looking (nadir) geometry right above the canopy under the simplified assumption of a nonscattering atmosphere, using a US standard atmosphere and 20 degree SZA. The top panel shows the incoming irradiance just above the canopy with absorptions of atmospheric oxygen (red), water vapor (blue), and Fraunhofer lines (black) separated. The middle panel shows typical reflectance curves for a canopy with an LAI of 3 but varying chlorophyll content from 5 to 40 μg/cm^2. The so-called red-edge with its sharp increase from 700 through 750 nm can be clearly distinguished and is the basis for most remotely sensed vegetation indices, which are often labeled with the misnomer "greenness indices." Here, the chlorophyll absorption feature is important for various reasons: (I) the red fluorescence peak at 680 nm undergoes re-absorption by chlorophyll, (II) the background reflectance is lower than at the far-red peak (740 nm), potentially making the derivation of SIF easier in this band; and (III) the red to far-red ratio also bears the potential to be a more direct indicator of plant stress but might be confounded with the impact of selective reabsorption. The lower panel shows the reflected radiance, i.e., the product of the two panels above using the 10 μg/cm^2 chlorophyll content and assuming a lambertian surface. The green curve indicates an SIF emission spectrum (scaled by 50), in this case taken from laboratory measurements derived using a blue LED as excitation light, which might overemphasize the red peak due to reduced reabsorption. The SIF emission spectrum shows the two distinct peaks at 685 and 740 nm, denoted as red and far-red peak, respectively.

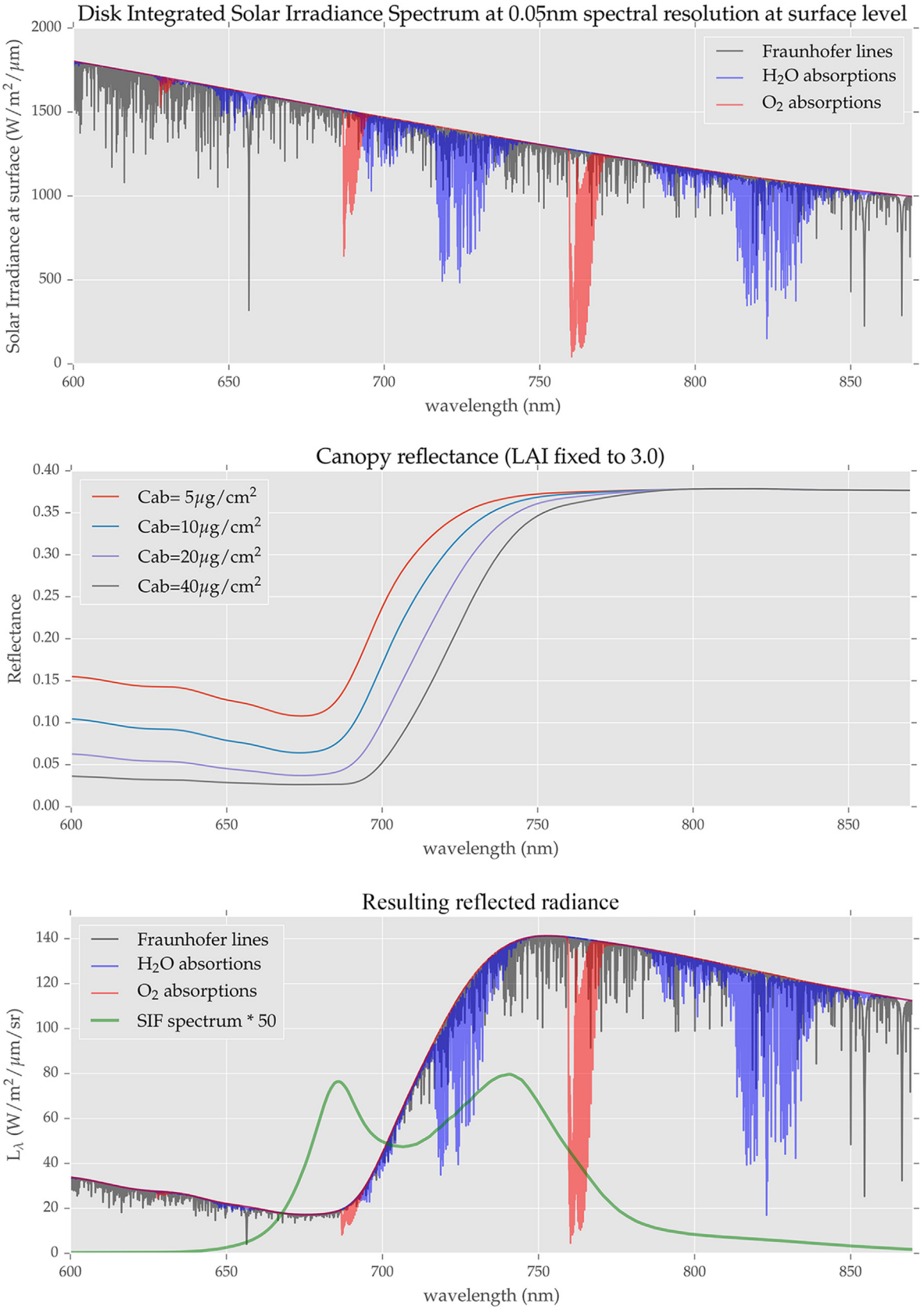

Fig. 9 This graph shows the main contributors to a reflectance spectrum observed at the top of canopy in nadir view. The *top panel* shows the incoming solar radiation including solar and telluric absorption features (assuming an US standard atmosphere and 20 degrees SZA). The *middle panel* show typical reflectance spectra for a variety of chlorophyll contents at a fixed LAI. The *bottom panel* shows the resulting reflected spectrum, including an assumed solar induced fluorescence emission (SIF, scaled by a factor 50) that is added.

To illustrate the impact of the small additive signal from SIF, we again rely on ratio spectra with and without added SIF. Contrary to the simple case study before, we have to take a more spectrally variable reflectance spectrum into account as well as a wavelength-dependent SIF signal. In addition, we now fully consider telluric absorptions within the Earth's atmosphere, but neglect atmospheric scattering for the sake of simplicity.

Fig. 10 shows the ratio between a spectrum with and without SIF right above the canopy. The impact on Fraunhofer lines and telluric O_2/H_2O features is separated by using different colors. Owing to the lower background reflectance, the relative SIF contribution in this case is much larger at the red peak, contributing up to 8% to the reflected radiance while only about 1% in the far red. Over the oceans, this broad "hump" around 685 nm is even more pronounced due to generally lower and well-defined ocean reflectance in nadir viewing with less water absorption than at the far red peak. This allows for the "hump" itself being used for the retrieval without the necessity for Fraunhofer lines and high-resolution spectrometers and thus can be achieved with band spectrometers such as MODIS, which use the normalized fluorescence line height (FLH, Letelier and Abbott 1996; Xing et al. 2007, and references therein) to infer chlorophyll fluorescence. This method simply calculates fluorescence as the difference between the observed and a linearly interpolated radiance at 678 nm, using two surrounding bands for interpolation. At longer wavelength, the SIF emission is more strongly absorbed by water and largely subdued but even the 678 nm SIF values is only emanating from the uppermost water-layer.

Over land, stronger variations of surface reflectances from different materials interfere with such an SIF retrieval approach. Thus, the information content of the overall SIF emission spectrum is largely reduced and we prefer to focus on the in-filling only. To

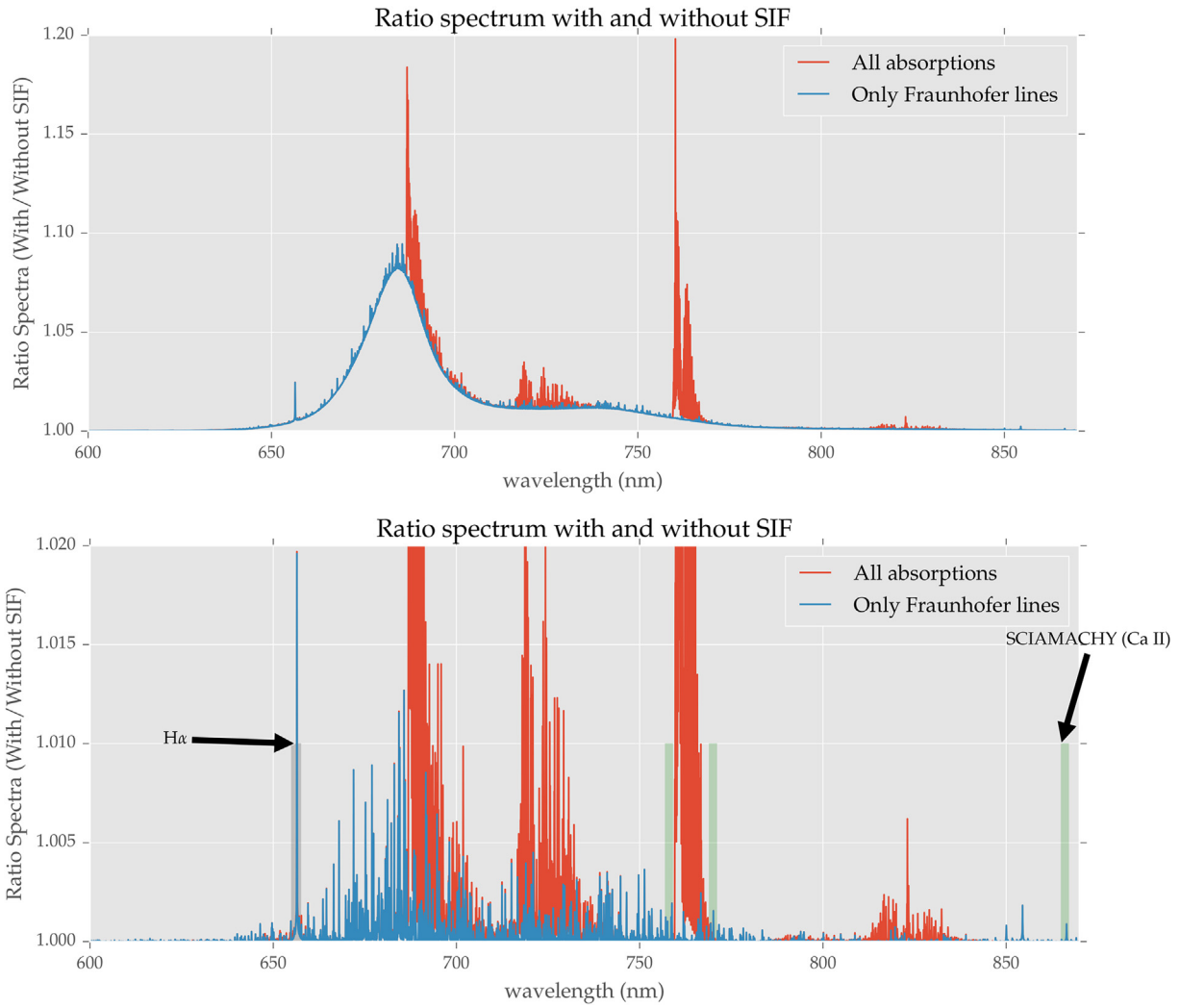

Fig. 10 This graph shows the impact of an spectrally variable SIF spectrum on the canopy reflectance by computing a ratio spectrum with and without the additive SIF signal. The *red curves* include both in-filling of H_2O as well as O_2 lines, while the *blue* ones only show the impact of Fraunhofer lines. In the *bottom-panel*, the impact of the broadband change in apparent reflectance is removed to focus on the high-frequent spectral variations, which is the primary way of retrieving SIF. A few specific spectral ranges that are currently being used for satellite-based SIF retrievals are noted by *green bars*.

illustrate this, we removed the effect on the broadband reflectance change in the lower panel, which only shows the degree of in-filling within the absorption features.

As mentioned before, we can use the "darker" parts of the spectrum to disentangle the additive offset from any multiplicative changes. The two main features in Fig. 10 are due to the oxygen absorption bands at 760 nm (O_2 A-band) and 685 nm (O_2 B-band), respectively, while the Fraunhofer lines appear less pronounced. This has to do with the depth of the absorption features, especially for the O_2 A-band, which is almost saturated and thus results in a much higher fractional signal change when a small signal is added. This is the primary reason the oxygen bands have been almost exclusively used in ground-based SIF studies. They provide two major advantages: (I) The absorption is much stronger, resulting in a higher in-filling and (II) the features are relatively wide (spectrally), not warranting as fine a spectral resolution as needed for Fraunhofer lines. The main disadvantage is that the depth of the oxygen bands can change due to other factors as well: for example, changes in the photon path-length distribution due to atmospheric scattering (Pfeilsticker et al., 1998; Funk and Pfeilsticker, 2003; Bril et al., 2007), changes in surface pressure as well as re-absorption by oxygen. These compounding factors increase with distance between the observer and vegetation as well as with the contribution of diffuse radiation.

If we focus on Fraunhofer lines only, there are currently two different retrieval strategies being employed. One is fully modeling a high-resolution synthetic solar model and uses the knowledge of the actual instrument line shape to generate modeled spectra, using a low-order polynomial to account for any multiplicative terms affecting the broadband continuum. In essence, this incorporates atmospheric and surface effects into a simple polynomial, which is sufficient at narrow fitting windows.

$$L^{\lambda}\left(SIF^{\lambda}, a\right) = SIF^{\lambda} + < I_0^{\lambda} > \cdot \sum_{i=0}^{n} a_i \cdot \lambda^i, \tag{8}$$

with $< >$ denoting the convolution with the instrument line-shape and sampling to the detector grid.

Usually, we assume a fixed SIF spectral shape, especially in the far red, which simplifies the SIF retrieval to a single scalar x, with $SIF^{\lambda} = x \cdot S_R^{\lambda}$, with S_R^{λ} being a reference spectral SIF shape, which can be normalized to 1 at the wavelength of interest, e.g., if $S_R\lambda$ is normalized to unity at 755 nm, x will directly provide SIF at 755 nm. The solution for $S1F^{\lambda}$ and all polynomial coefficients in a given a measurement vector γ^{λ} is then provided in a least squares fit, minimizing the squared differences between modeled and measured spectra, weighted by their respective $1-\sigma$ random noise, which constitute the purely diagonal measurement error covariance matrix $S_{\varepsilon}^{\lambda}$:

$$X^2 = \left(L^{\lambda}\left(SIF^{\lambda}, a\right) - \gamma^{\lambda}\right)^T S_{\varepsilon}^{\lambda}\left(L^{\lambda}\left(SIF^{\lambda}, a\right) - \gamma^{\lambda}\right). \tag{9}$$

Solving the least squares problem yields the optimized SIF estimate as well as polynomial coefficients. It also provides the proper posterior error statistics, especially if there is good knowledge of $S_{\varepsilon}^{\lambda}$. In the most general case, the forward model also includes fit parameters for the spectral calibration, i.e., spectral shift and squeeze parameters. Even if the fit is performed in log(radiance) space, as was proposed by (Frankenberg et al. (2011a), the spectral shift fits render the problem nonlinear, in which case the solution has to be found in an iterative way.

Another similar approach has been initially developed by Guanter et al. (2012), using a singular value decomposition (SVD) of spectra from a *training dataset*, which is ideally devoid of SIF. This yields a set of orthogonal basis vectors that constitute a typical spectral observation. The advantage of this approach is that it is a *data-driven retrieval*, which does not require exact knowledge of the instrument lineshape and spectral sampling, which were all included in the convolution term $< >$. With the SVD approach, the observed radiation with SIF can be fitted using a linear combination of the basis vectors as well as the SIF signal:

$$L^{\lambda}(SIF^{\lambda}, \omega) = \sum_{i=1}^{n} \omega_i v_i^{\lambda} + SIF^{\lambda}, \tag{10}$$

with SIF^{λ} being modeled as the product of a fixed reference shape with a scalar, as mentioned before. In this case, v_i^{λ} represent the basis vectors derived using the SVD of the training dataset and w_i the weighting factors that can be derived using linear least-squares. This technique effectively fits some of the instrument properties as well and the first singular vector usually represents an average spectrum of reflected light while the remaining ones can shed light on wavelength-dependent structures and instrument-related effects such as spectral shifts or etalon effects. Similar to the full fitting approach, this SVD method has been applied to ground-based observations as well as space-based retrievals not covering spectral regions with telluric absorption features.

Instruments such as GOME-2 and SCIAMACHY have a far lower spectral resolution than GOSAT and OCO-2 and thus preclude the application of very narrow microwindows using spectral ranges devoid of telluric absorption features. In addition, the lower spectral resolution would result in higher retrieval noise using small windows. Thus, there was a need to include wider spectral ranges in SIF fitting methods, which would then need to account for atmospheric absorptions. Modifications to account for telluric absorptions have enable this *data-driven retrieval* to be applied to various other satellites, which features a lower spectral resolution (>0.2 nm) but enable full global sampling as well as better revisit times. For the top-of-atmosphere radiance, the SVD-based forward model (Joiner et al., 2013; Köhler et al., 2015; Guanter et al., 2015; Sanders et al., 2016) reads

$$L^{\lambda}\left(SIF^{\lambda}, w\right) = \sum_{i=1}^{n_1}\left(a_i\lambda_i\right) \cdot \sum_{j=1}^{n_2}\left(w_i v_i^{\lambda}\right) + SIF^{\lambda} \cdot T_{\uparrow}, \tag{11}$$

which is analogous to Eq. 10 but includes the transmission term for the upward fluorescence $T_{\uparrow}$ as well as an additional polynomial term in wavelength, which can change the overall shape of the contribution from the fitted singular vectors w_i. Typically, n_1 is of low

order (2–3) and recent methods only use the polynomial scaling for the first eigenvector, not all. The most important factor to note is that instead of using radiative transfer calculations, this approach folds in all radiative transfer aspects into the eigenvectors w_i, which are generated using either simulated radiances or real satellite data. This requires an extensive set of simulated data or real satellite data, covering as variable atmospheric conditions as possible over nonfluorescing targets (see details in Joiner et al. 2013; Köhler et al. 2015; Guanter et al. 2015). The major advantage of this approach is that it enables the use of a much wider fitting window, which can include telluric absorption features such as the oxygen bands or water bands. However, it is important to note that information for the SIF retrieval itself is mostly coming from the Fraunhofer lines. This approach is the corner stone for many global retrievals right now and will also be applicable to TROPOMI satellite data, which will provide an unprecedented dataset in terms of spatial resolution and revisit time (Guanter et al., 2015).

3.10.5 Additional Challenges from Space

So far, we have ignored atmospheric scattering and absorption, mostly because the depth of the Fraunhofer lines is, with the exception of the impact of rotational Raman scattering (Grainger and Ring, 1962a; Chance and Spurr, 1997), invariant to these effects, which alter spectra in a multiplicative way only. However, scattering and absorption is very crucial when SIF retrievals from afar are attempted. The *data-driven* SVD-based retrieval accounted for these effects using the eigenvector w_i but here we focus on what additional challenges are occurring in general.

Fig. 11 shows the impact of reabsorption by both H_2O as well as O_2 at different observing altitudes. The effect of H_2O in this case is likely largely underestimated as we assumed only 10% of the total column water to be present in the lowermost 10 km, while in reality, it exceeds 50%. One can already see that the SIF signal is heavily attenuated in the telluric absorption bands, which now may also be partially filled in by atmospheric scattering. On the other hand, in spectral areas devoid of atmospheric absorption, the SIF signal is unperturbed. There are additional complications, namely, how does the in-filling really look like under realistic conditions from space and how much of the fluorescence emanating from the top of canopy actually reaches the top of atmosphere.

This effect can only be quantified using full multiple-scattering radiative transfer simulations. Here, we used a few simulations from the orbit simulator (O'Brien et al., 2009) for the Orbiting Carbon Observatory, which includes realistic aerosol and cloud distributions as well as a fluorescence. The simulator provides a realistic representation of the fluorescence emission, which also undergoes scattering in the atmosphere (Frankenberg et al., 2012). A few examples are discussed here for illustration. Fig. 12 shows results from the orbit simulator for three different cases with very low, moderate, and high extinction optical depths in the atmosphere: 0.1, 0.32, and 2.1, respectively. The top panel shows the effect of SIF at the TOA using ratio spectra of scene simulations with and without fluorescence added, with all other parameters kept constant. The most dramatic effect is that the 10%–20% infilling observed on the ground is largely diminished to about 1%. For ground-based observations, each observed photon traversed the entire atmosphere in the downward direction before detection, while this is not true for observations from space. Especially in the deep absorption lines of the oxygen band, many photons are being back-scattered due to Rayleigh, aerosol, or cloud scattering. In these cases, photons of different wavelengths in fact have a different photon-pathlength distribution within the atmosphere, giving rise to changes in the spectral shape of the oxygen band. This is the primary reason the oxygen bands are being measured to account for light path changes in accurate measurements of atmospheric greenhouses

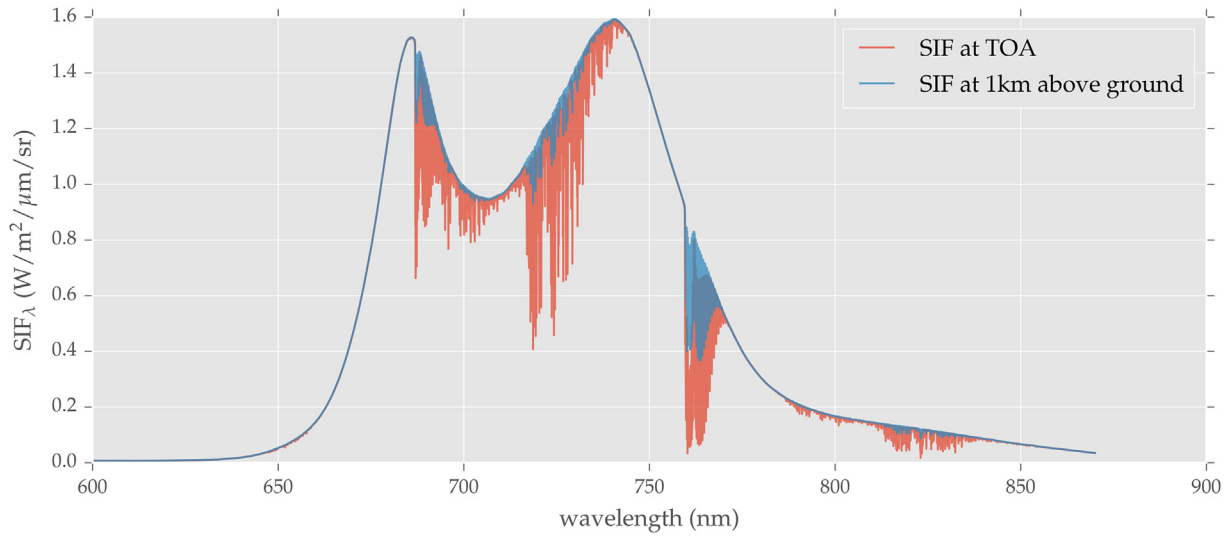

Fig. 11 This graph shows the impact of reabsorption on the fluorescence signal at different observing altitudes (1 km and top of atmosphere).

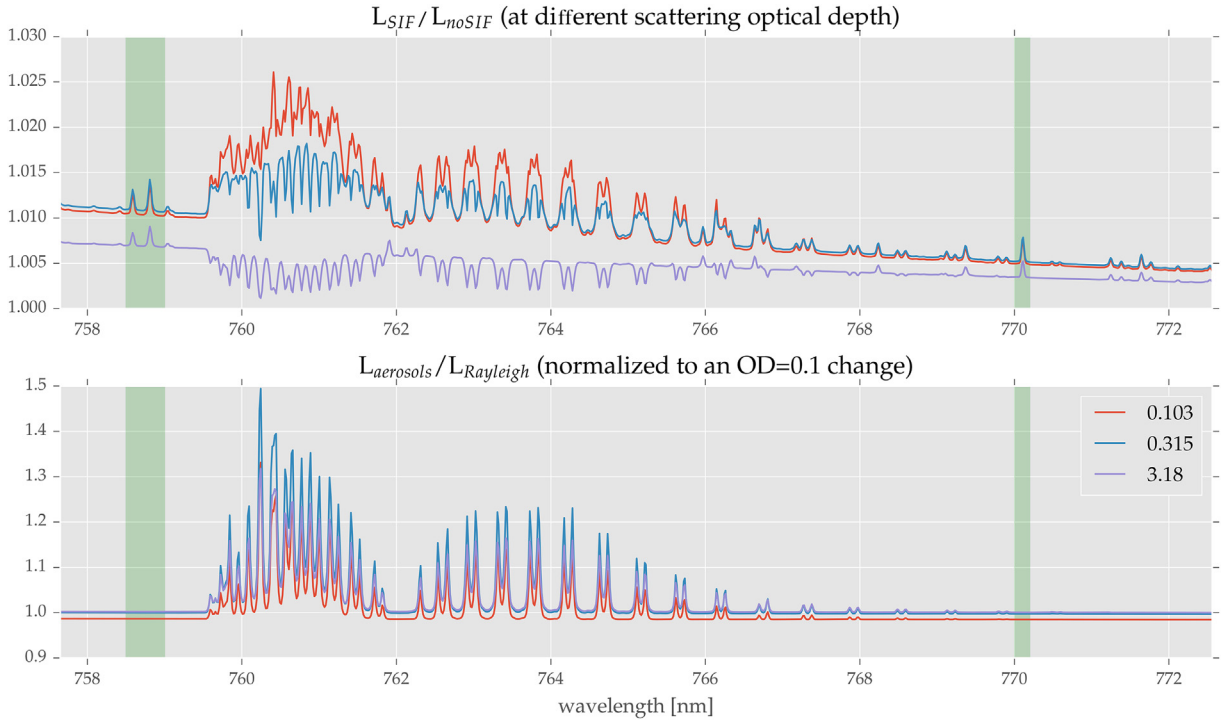

Fig. 12 *Top*: Results from the OCO_2 orbit simulator using three tropical observations with varying optical depths (due to aerosols as well as water and ice clouds). The ratio depicts the modeled OCO_2 observed radiance with (L_{SIF}) and without (L_{noSIF}) added SIF. In the *bottom*, we contrast the effect or atmospheric scattering on the in-filling by showing the ratio of the full radiative transfer run with added scattering optical depth ($L_{aerosols}$) as well as in a pure Rayleigh atmosphere ($L_{Rayleigh}$). The changes in the bottom panel have been normalized to an optical depth change of 0.1 and scaled to about 1 in the continuum.

gases (Bösch et al., 2006; Butz et al., 2009; O'Dell et al., 2011). An extreme example is the high optical depth case, where the added SIF actually causes an increase in the O_2 absorption depth rather than a decrease. This may appear counterintuitive but can be explained by the different photon path-length distributions taken by solar photons as opposed to those emitted from vegetation. In optically thick atmospheres, the amount of O_2 absorptions in back-scattered light might be lower than from SIF, which must by definition have at least traversed the entire geometric light path from the vegetation to the top of atmosphere. In this case, the SIF contribution includes deeper O_2 lines than the observations without SIF. The ratio spectrum is still >1 by definition, but the sign of the in-filling can be swapped.

However, this may be an extreme case, which can be discarded using cloud filters. However, the dramatic advantage of using the oxygen lines diminishes from space. For reference, the lower panel shows the effect of scattering on the O_2 absorption lines by computing the ratio from the simulations with aerosols added and with a pure Rayleigh only atmosphere. This effect has been scaled to show just the effect of a change in the optical depths of 0.1 but still dwarfs the magnitude caused by SIF by about a factor 10. The major challenge from space is to really disentangle atmospheric scattering from the effect of SIF. Using only the O_2 A-band, this can be ambiguous and an under-determined numerical problem (Frankenberg et al., 2011a). Using a wider spectral range and including the O_2-B band might increase the information content (Guanter et al., 2010b; Sanghavi et al., 2012), similar to recent advances using the $O_2\gamma$ band to constrain scattering properties for the retrieval of red fluorescence (Joiner et al., 2016).

On the other hand, the Fraunhofer line method is rather insensitive to atmospheric scattering and would even work in the high optical density case. In addition, it is computationally much easier as extensive radiative transfer computations can be avoided.

Fig. 13 shows an additional advantage of using the Fraunhofer line method from space. As this method is not affected by telluric re-absorption, the fraction of SIF reaching the top of atmosphere is not heavily affected by atmospheric scattering if the single scattering albedo is close to 1. Under this scenario, most SIF radiation emitted at the surface still propagates through the atmosphere, even in the presence of clouds, which act as a diffusor rather than fully blocking the emitted radiation from the surface. This is an entirely different situation from reflectance-based methods, such as vegetation indices, which can be heavily perturbed by atmospheric scattering and are impossible to retrieve under cloudy conditions. SIF, on the other hand, is really an emission from the surface, more akin to city lights at night seen from an aircraft (or satellite) at higher altitude. Everyone who observed city lights from an aircraft through moderately thick clouds or haze would have experienced this. In Fig. 13, we show the fraction of SIF at the TOA that is reaching the detector in a realistic atmosphere as opposed to a completely cloud and aerosol-free scene (with only Rayleigh scattering present). Even at optical depths of 3–4, about 80% of the SIF radiation is still reaching the top of atmosphere, indicating that SIF can still be retrieved in scattering atmospheres. In principle, this reduction in SIF reaching the TO A

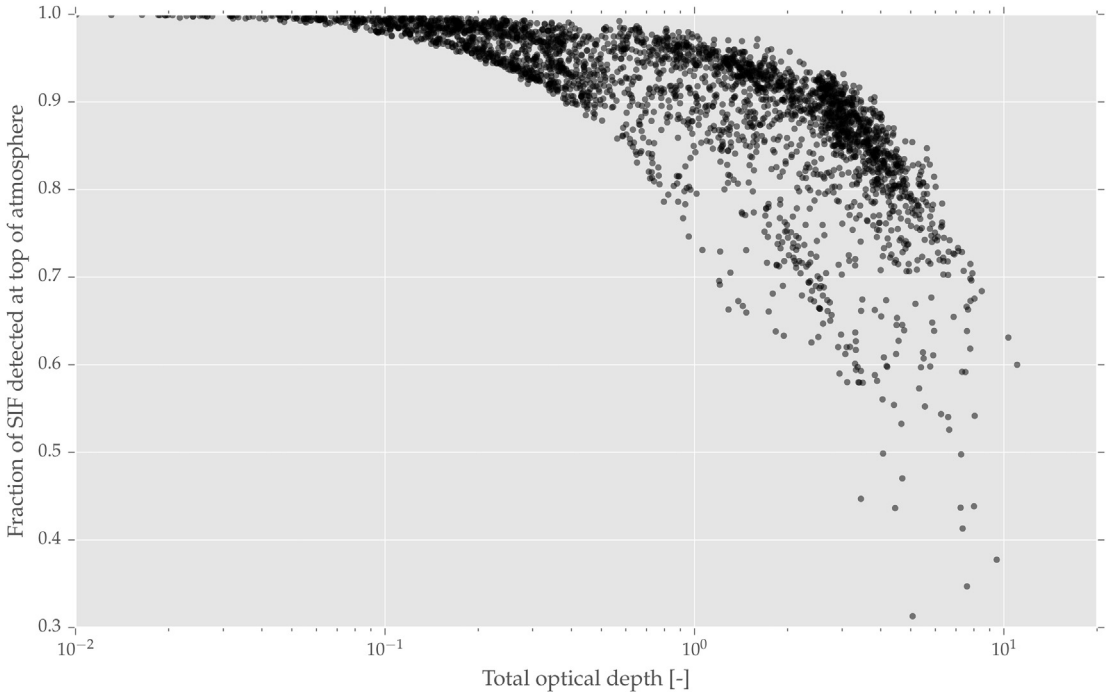

Fig. 13 This graph shows the fraction of SIF actually observed at the top of atmosphere in the present of clouds and aerosols with various optical depths. In almost all simulations, more than 60% of the emitted SIF can actually be detected using the Fraunhofer line method. Most often, about 80%–90% reach the top of atmosphere even at optical depths of 3–4. Strict cloud filtering is thus not as critical as for reflectance-based remote sensing.

should be proportional to the fraction of potential PAR radiation reaching the top of canopy. This would allow us to more closely study the impact of atmospheric scattering and diffuse radiation on photosynthesis and SIF emissions.

3.10.5.1 Notes on Quality Control

While the SIF retrieval using oxygen absorptions from ground-based measurements or Fraunhofer lines from the ground or in space is fairly straightforward, there are various factors that could affect the accuracy and precision. So far, no standards have been developed to homogenize SIF retrievals. As most groups use different instrument and observation strategies, it is hard to provide universal guidance, but we want to explain some of the common factors to be cognizant about. For virtually all of the Fraunhofer-based retrievals, we realized that the retrievals tell us as much about the instrument as about SIF itself and these two aspects need to be disentangled.

For instance, SIF retrievals for both GOSAT and OCO-2 helped detect a zero-level offset in the Fourier Transform Spectrometer data acquisition (GOSAT) and a time-dependent stray-light issue due to an ice-layer buildup in front of the detector array for OCO-2. Similar considerations hold for GOME-2 and SCIAMACHY as well (Joiner et al., 2012; Köhler et al., 2015). Both effects can mimic SIF as they have exactly the same effect on the depths of Fraunhofer lines as SIF. Thus, it is necessary to use nonfluorescing reference targets to disentangle the in-filling due to instrumental effects and SIF. In addition, the zero-level offset effect in FTS systems is signal level dependent, requiring a characterization of the instrument related in-filling as a function of signal level. The same holds for the effect of potential detector nonlinearities in regular grating spectrometers. Quality control using reference targets at the full dynamic range of signal levels is thus indispensable. In particular, the signal-level-dependent bias can be very crucial as the reflectance at 750 nm also correlates with greenness indices, which could result in spurious correlations between absolute SIF and greenness indices. In ground-based systems, there is a simple way around this major error by not using a constant detector integration time: The integration time can be constantly adjusted so that the raw detector readout level remains constant in the retrieval window of interest. The dark current also has to be properly characterized as it constitutes an additive offset as well and could be confused with SIF as well.

In addition, illumination effects can have a large impact as the total SIF will depend on the fraction of directly illuminated leaves, which correlates with the absolute radiance in the far red as well. Hence, studies of both absolute SIF as well as relative SIF (SIF divided by continuum radiance) can often be illuminating. If Fraunhofer lines are used, one can also make use of the strong wavelength dependence of SIF to disentangle it from other factors that might have a flat response, such as dark current or stray-light. It is very important to fully understand the SIF retrievals, instrumental effects as well as observational geometries and the robustness of the retrievals before interpreting the data. Most crucial are errors that might depend on absolute signal level.

In summary, there are many instrument effects that have the same effect as an additive offset and can thus not be easily disentangled from a real SIF signal in the absence of its proper characterization using reference targets. These effects range from a zero-level offset in FTS system, and detector nonlinearities in grating spectrometers to simple dark current biases or spectral and spatial straylight. To avoid the latter, the use of band-pass or at least long-pass filters is encouraged to minimize straylight from other spectral regions and effectively eliminate order overlap in grating spectrometer systems.

Regarding the use of oxygen lines in ground-based retrievals, a few more aspects should be considered. First, the reabsorption of SIF has to be considered when the detector is further away from the SIF emission. In addition, the O_2 absorption depth of direct sunlight will be different from atmospheric straylight. If a shaded fraction of a canopy is observed, this might result in a spurious SIF retrieval when a directly illuminated reference target is used for the retrieval. We suggest to carefully study the magnitude of these potential effects using reference targets in similar illumination conditions (direct and shaded/diffuse).

3.10.6 Conclusions and Outlook

Recent space-borne observations of solar-induced chlorophyll fluorescence as well as the selection of FLEX, the first dedicated space-borne SIF mission, have stimulated a new focus on fluorescence from the planet. Initial empirical studies point to a linear correlation with gross primary production (GPP) (Frankenberg et al., 2011b), prompting numerous follow-up studies using SIF as a GPP proxy. While we see an immense potential in using SIF as a GPP proxy, we caution that the empirical findings somewhat contradict measurements of light response curves of individual leaves, where GPP saturates while SIF does not, resulting in somewhat nonlinear relationship between GPP and SIF on the leaf level. However, retrievals from a sun-synchronous satellite would tend to be under similar illumination conditions, so the nonlinearity might not be important. Strictly speaking, Eqs. 3 and 4 hold for individual leaves and need to be integrated over all leaves within a canopy at a variety of incident levels of PAR, potentially linearizing some of the nonlinearities occurring on the individual leaf level (Zhang et al., 2016).

A few models now include forward-modeling of SIF (Tol et al., 2009, 2014; Lee et al., 2015) but rely on different empirical parameterizations of the fluorescence yield as a function of the photosynthesis yield, computed using the Farquhar/von Caemmerer/Berry photosynthesis model (Farquhar et al., 1980). These parameterizations are based on a limited set of leaf-level data and often fail under specific conditions such as sustained quenching in evergreen needle-leaf forests in winter. In addition, the relative contributions of PSI and PSII as well as their spectral shapes that constitute the total SIF signal are still debated. The bridge between remote sensing science and the photosynthesis research community is bringing theory, more quantitative approaches, and analysis of scale into the remote sensing world, and on the other side, it is bringing a global perspective to what has largely been a laboratory-based science. This can only be good for both disciplines.

In terms of SIF retrievals, we will have to ensure a rigid quality control, especially with the proliferation of new SIF measurements using existing or new ground-based devices. While the Fraunhofer-lines-based method is in principle trivial, several instrumental features can confound the retrievals and need to be well understood. When using O_2 absorption features, the caveats related to atmospheric scattering and differences in direct versus diffuse incident light need to be fully characterized. One of the main challenges is a calibration standard as there are no other ways of measuring SIF. Fs from PAM measurements is not absolute-radiometrically calibrated and can only be used to study relative variations, while absolute Fs values are impacted by the amount of absorbed light as well. The best we can do at the moment are calibration targets, which are known to be nonfluorescing to evaluate the zero baseline. Ideally, these targets should be observed at different illumination and absolute brightness conditions, similar to actual vegetation. For applications using a reference target, additional zero-level targets of different materials not used in the training dataset could be used.

Acknowledgments

We thank Joanna Joiner, Phillip Köhler, and Luis Guanter for valuable input and proofreading of the manuscript. We thank C.W. O'Dell and T.E. Taylor from the Cooperative Institute for Research in the Atmosphere of the Colorado State University for providing the OCO-2 orbit simulator data used in the analysis of the scattering impact. We have to acknowledge that the writing of this article had to be rushed and sincerely apologize beforehand for any potential omissions or inaccuracies related to a lack of time. Given the very extensive amount of fluorescence-related literature, we certainly might have missed to cite some of the relevant papers.

See also: 3.11. Vegetation Primary Productivity.

References

Badgley, G., Field, C. B., & Berry, J. A. (2017). Canopy near-infrared reflectance and terrestrial photosynthesis. *Science Advances*, *3*(3). http://dx.doi.org/10.1126/sciadv.1602244. e1602244.

Baker, N. R. (2008). Chlorophyll fluorescence: A probe of photosynthesis in vivo. *Annual Review of Plant Biology*, *59*, 89–113.

Björkman, O., & Demmig, B. (1987). Photon yield of O_2 evolution and chlorophyll fluorescence characteristics at 77 K among vascular plants of diverse origins. *Planta, 170*(4), 489–504.

Blankenship, R. E. (2013). *Molecular mechanisms of photosynthesis*. Chichester: John Wiley & Sons.

Bösch, H., Toon, G. C., Sen, B., Washenfelder, R. A., Wennberg, P. O., Buchwitz, M., de Beek, R., Burrows, J. P., Crisp, D., & Christi, M. (2006). Space-based near-infrared CO_2 measurements: Testing the Orbiting Carbon Observatory retrieval algorithm and validation concept using SCIA-MACHY observations over Park Falls, Wisconsin. *Journal of Geophysical Research, 111*, 0148–0227.

Bril, A., Oshchepkov, S., Yokota, T., & Inoue, G. (2007). Parameterization of aerosol and cirrus cloud effects on reflected sunlight spectra measured from space: Application of the equivalence theorem. *Applied Optics, 46*, 2460–2470.

Brinkmann, R. T. (1968). Rotational raman scattering in planetary atmospheres. *The Astrophysical Journal, 154*, 1087.

Buschmann, C. (2007). Variability and application of the chlorophyll fluorescence emission ratio red/far-red of leaves. *Photosynthesis Research, 92*(2), 261–271.

Butz, A., Hasekamp, O. P., Frankenberg, C., & Aben, I. (2009). Retrievals of atmospheric CO_2 from simulated space-borne measurements of backscattered near-infrared sunlight: Accounting for aerosol effects. *Applied Optics, 48*(18), 3322–3336.

Campbell, P. K. E., Middleton, E. M., McMurtrey, J. E., Chappelle, E. W., et al. (2007). Assessment of vegetation stress using reflectance or fluorescence measurements. *Journal of Environmental Quality, 36*(3), 832–845.

Chance, K. V., & Spurr, R. J. D. (1997). Ring effect studies: Rayleigh scattering, including molecular parameters for rotational raman scattering, and the fraunhofer spectrum. *Applied Optics, 36*(21), 5224–5230.

Crisp, D., Meadows, V. S., Bezard, B., de Bergh, C., Maillard, J.-P., & Mills, F. P. (1996). Ground-based near-infrared observations of the venus nightside: 1.27-μm o_2 (a $1\delta g$) airglow from the upper atmosphere. *Journal of Geophysical Research, Planets, 101*(E2), 4577–4593.

Damm, A., Elbers, J., Erler, A., Gioli, B., Hamdi, K., Hutjes, R., Kosvancova, M., Meroni, M., Migli-Etta, F., Moersch, A., Moreno, J., Schick-Ling, A., Sonnenschein, R., Udelhoven, T., Van Der Linden, S., Hostert, P., & Rascher, U. (2010). Remote sensing of sun-induced fluorescence to improve modeling of diurnal courses of gross primary production (gpp). *Global Change Biology, 16*(1), 171–186. http://dx.doi.org/10.1111/j.1365-2486.2009.01908.x. ISSN 1365–2486.

Demmig, B., & Björkman, O. (1987). Comparison of the effect of excessive light on chlorophyll fluorescence (77 k) and photon yield of o_2 evolution in leaves of higher plants. *Planta, 171*(2), 171–184.

Drusch, M., Moreno, J., Del Bello, U., Franco, R., Goulas, Y., Huth, A., Kraft, S., Middleton, E. M., Miglietta, F., Mohammed, G., et al. (2016). The fluorescence explorer mission concept-esa's earth explorer 8. *IEEE Transactions on Geoscience and Remote Sensing, 55*, 1273–1284.

Farquhar, G. D., von Caemmerer, S., & Berry, J. A. (1980). A biochemical model of photosynthetic CO_2 assimilation in leaves of c3 species. *Planta, 149*(1), 78–90.

Flexas, J., Mariano Escalona, J., Evain, S., Gulías, J., Moya, I., Barry Osmond, C., & Medrano, H. (2002). Steady-state chlorophyll fluorescence (fs) measurements as a tool to follow variations of net CO_2 assimilation and stomatal conductance during water-stress in c3 plants. *Physiologia Plantarum, 114*(2), 231–240.

Frankenberg, C., Butz, A., & Toon, G. C. (2011). Disentangling chlorophyll fluorescence from atmospheric scattering effects in o-2 a-band spectra of reflected sun-light. *Geophysical Research Letters, 38*, L03801. http://dx.doi.org/10.1029/2010GL045896. http://www.agu.org/pubs/crossref/2011/2010GL045896.shtml.

Frankenberg, C., Fisher, J., Worden, J., Badgley, G., Saatchi, S., Lee, J., Toon, G., Butz, A., Jung, M., Kuze, A., & Yokota, T. (2011). New global observations of the terrestrial carbon cycle from gosat: Patterns of plant fluorescence with gross primary productivity. *Geophysical Research Letters, 38*(17), L17706. http://dx.doi.org/10.1029/2011GL048738.

Frankenberg, C., O'Dell, C., Guanter, L., McDuffie, J., & 2081–2094. (2012). Remote sensing of near-infrared chlorophyll fluorescence from space in scattering atmospheres: Implications for its retrieval and interferences with atmospheric CO_2 retrievals. *Atmospheric Measurement Techniques, 5*(8), 2081–2094. http://dx.doi.org/10.5194/amt-5-2081-2012. http://www.atmos-meas-tech.net/5/2081/2012/.

Frankenberg, C., O'Dell, C., Berry, J., Guanter, L., Joiner, J., KÃűhler, P., Pollock, R., & Taylor, T. E. (2014). Prospects for chlorophyll fluorescence remote sensing from the orbiting carbon observatory-2. *Remote Sensing of Environment, 147*, 1–12. http://dx.doi.org/10.1016/j.rse.2014.02.007. ISSN 0034–4257.

Freedman, A., Cavender-Bares, J., Kebabian, P. L., Bhaskar, R., Scott, H., & Bazzaz, F. A. (2002). Remote sensing of solar-excited plant fluorescence as a measure of photosynthetic rate. *Photosynthetica, 40*(1), 127–132.

Funk, O., & Pfeilsticker, K. (2003). Photon path length distributions for cloudy skies? Oxygen A-Band measurements and model calculations. *Annales Geophysicae, 21*(3), 615–626.

Genty, B., Briantais, J.-M., & Baker, N. R. (1989). The relationship between the quantum yield of photosynthetic electron transport and quenching of chlorophyll fluorescence. *Biochimica et Biophysica Acta (BBA)-General Subjects, 990*(1), 87–92.

Gitelson, A. A., Buschmann, C., & Lichtenthaler, H. K. (1999). The chlorophyll fluorescence ratio f735/f700 as an accurate measure of the chlorophyll content in plants. *Remote Sensing of Environment, 69*(3), 296–302.

Govindjee. (2012). *Energetics of photosynthesis*. Burlington: Elsevier.

Grainger, J. F., & Ring, J. (1962). Anomalous Fraunhofer line profiles. *Nature, 193*, 762.

Grainger, J. F., & Ring, J. (1962). The luminescence of the lunar surface. In Z. Kopal (Ed.), *Physics and astronomy of the moon* (pp. 385–405). New York and London: Academic Press.

Grainger, J. F., & Ring, J. (1962). *Lunar luminescence*. In *In: vol. 14,* Symposium-International Astronomical Union (vol. 14, pp. 445–452). Cambridge: Cambridge University Press.

Guan, K., Pan, M., Li, H., Wolf, A., Wu, J., Medvigy, D., Caylor, K. K., Sheffield, J., Wood, E. F., Malhi, Y., et al. (2015). Photosynthetic seasonality of global tropical forests constrained by hydroclimate. *Nature Geoscience, 8*(4), 284–289.

Guan, K., Berry, J. A., Zhang, Y., Joiner, J., Guanter, L., Badgley, G., & Lobell, D. B. (2016). Improving the monitoring of crop productivity using spaceborne solar-induced fluorescence. *Global Change Biology, 22*(2), 716–726. http://dx.doi.org/10.1111/gcb.13136.

Guanter, L., Alonso, L., Gómez-Chova, L., Amorós-López, J., Vila, J., & Moreno, J. (2007). Estimation of solar-induced vegetation fluorescence from space measurements. *Geophysical Research Letters, 34*(8), L08401.

Guanter, L., Alonso, L., Gómez-Chova, L., Meroni, M., Preusker, R., Fischer, J., & Moreno, J. (2010a). Developments for vegetation fluorescence retrieval from spaceborne high-resolution spectrometry in the O_2-A and O_2-B absorption bands. *Journal of Geophysical Research, 115*(D19), D19303. http://dx.doi.org/10.1029/2009JD013716.

Guanter, L., Alonso, L., Ãşmez-Chova, G., et al. (2010b). Developments for vegetation fluorescence retrieval from spaceborne high-resolution spectrometry in the O_2-a and O_2-b absorption bands. *Journal of Geophysical Research: Atmospheres, 115*(D19), 2156–2202. http://dx.doi.org/10.1029/2009JD013716.

Guanter, L., Frankenberg, C., Dudhia, A., Lewis, P. E., Gómez-Dans, J., Kuze, A., Suto, H., & Grainger, R. G. (2012). Retrieval and global assessment of terrestrial chlorophyll fluorescence from GOSAT space measurements. *Remote Sensing of Environment, 121*, 236–251.

Guanter, L., Zhang, Y., Jung, M., Joiner, J., Voigt, M., Berry, J. A., Frankenberg, C., Huete, A. R., Zarco-Tejada, P., Lee, J.-E., et al. (2014). Global and time-resolved monitoring of crop photosynthesis with chlorophyll fluorescence. *Proceedings of the National Academy of Sciences, 111*(14), E1327–E1333.

Guanter, L., Aben, I., Tol, P., Krijger, J. M., Hollstein, A., Köhler, P., Damm, A., Joiner, J., Frankenberg, C., & Landgraf, J. (2015). Potential of the tropospheric monitoring instrument (tropomi) onboard the sentinel-5 precursor for the monitoring of terrestrial chlorophyll fluorescence. *Atmospheric Measurement Techniques, 8*(3), 1337–1352. http://dx.doi.org/10.5194/amt-8-1337-2015.

Iermak, I., Vink, J., Bader, A. N., Wientjes, E., & van Amerongen, H. (2016). Visualizing heterogeneity of photosynthetic properties of plant leaves with two-photon fluorescence lifetime imaging microscopy. *Biochimica et Biophysica Acta-Bioenergetics, 1857*(9), 1473–1478.

Jeong, S., Schimel, D., Frankenberg, C., Drewry, D. T., Fisher, J. B., Verma, M., Berry, J. A., Lee, J., & Joiner, J. (2017). Application of satellite solar-induced chlorophyll fluorescence to understanding large-scale variations in vegetation phenology and function over northern high latitude forests. *Remote Sensing of Environment, 190*, 178–187. http://dx.doi.org/10.1016/j.rse.2016.11.021.

Joiner, J., Bhartia, P. K., Cebula, R. P., Hilsenrath, E., McPeters, R. D., & Park, H. (1995). Rotational raman scattering (ring effect) in satellite backscatter ultraviolet measurements. *Applied Optics, 34*(21), 4513–4525.

Joiner, J., Yoshida, Y., Vasilkov, A. P., Yoshida, Y., Corp, L. A., & Middleton, E. M. (2011). First observations of global and seasonal terrestrial chlorophyll fluorescence from space. *Biogeosciences, 8*(3), 637–651. http://dx.doi.org/10.5194/bg-8-637-2011.

Joiner, J., Yoshida, Y., Vasilkov, A. P., Middleton, E. M., Campbell, P. K. E., Yoshida, Y., Kuze, A., & Corp, L. A. (2012). Filling-in of near-infrared solar lines by terrestrial fluorescence and other geophysical effects: Simulations and space-based observations from sciamachy and gosat. *Atmospheric Measurement Techniques, 5*(4), 809–829. http://dx.doi.org/10.5194/amt-5-809-2012.

Joiner, J., Guanter, L., Lindstrot, R., Voigt, M., Vasilkov, A. P., Middleton, E. M., Huemmrich, K. F., Yoshida, Y., & Frankenberg, C. (2013). Global monitoring of terrestrial chlorophyll fluorescence from moderate-spectral-resolution near-infrared satellite measurements: Methodology, simulations, and application to gome-2. *Atmospheric Measurement Techniques, 6*(10), 2803–2823. http://dx.doi.org/10.5194/amt-6-2803-2013.

Joiner, J., Yoshida, Y., Guanter, L., & Middleton, E. M. (2016). New methods for the retrieval of chlorophyll red fluorescence from hyperspectral satellite instruments: Simulations and application to gome-2 and sciamachy. *Atmospheric Measurement Techniques, 9*(8), 3939–3967. http://dx.doi.org/10.5194/amt-9-3939-2016.

Kattawar, G. W., Young, A. T., & Humphreys, T. J. (1981). Inelastic scattering in planetary atmospheres. I-the ring effect, without aerosols. *The Astrophysical Journal, 243*, 1049–1057.

Kautsky, H. (1931). Energie-umwandlungen an grenzflächen, iv. mitteil.: H. kautsky und a. hirsch: Wechselwirkung zwischen angeregten farbstoff-molekülen und sauerstoff. *European Journal of Inorganic Chemistry, 64*(10), 2677–2683.

Khosravi, N., Vountas, M., Rozanov, V. V., Bracher, A., Wolanin, A., & Burrows, J. P. (2015). Retrieval of terrestrial plant fluorescence based on the in-filling of far-red fraunhofer lines using SCIAMACHY observations. *Frontiers in Environmental Science, 3*(78). http://dx.doi.org/10.3389/fenvs.2015.00078. ISSN 2296-665X.

Koffi, E. N., Rayner, P. J., Norton, A. J., Frankenberg, C., & Scholze, M. (2015). Investigating the usefulness of satellite derived fluorescence data in inferring gross primary productivity within the carbon cycle data assimilation system. *Biogeosciences Discussions, 12*(1), 707–749.

Köhler, P., Guanter, L., & Joiner, J. (2015). A linear method for the retrieval of sun-induced chlorophyll fluorescence from gome-2 and sciamachy data. *Atmospheric Measurement Techniques, 8*(6), 2589–2608. http://dx.doi.org/10.5194/amt-8-2589-2015.

Kozyrev, N. A. (1956). Luminescence of the lunar surface and intensity of corpuscular radiation of the sun. *Proceedings of the Crimean Astron. Observatory, 16*, 148–158.

Krause, G. H., & Weis, E. (1984). Chlorophyll fluorescence as a tool in plant physiology. *Photosynthesis Research, 5*(2), 139–157.

Krause, G. H., & Weis, E. (1991). Chlorophyll fluorescence and photosynthesis—the basics. *Annual Review of Plant Physiology, 42*, 313–349.

Lee, J.-E., Frankenberg, C., Tol, C.v.d., Berry, J. A., Guanter, L., Kevin Boyce, C., Fisher, J. B., Morrow, E., Worden, J. R., Asefi, S., et al. (2013). Forest productivity and water stress in Amazonia: Observations from gosat chlorophyll fluorescence. *Proceedings of the Royal Society of London B: Biological Sciences, 280*(1761), 20130171.

Lee, J.-E., Berry, J. A., Tol, C., Yang, X., Guanter, L., Damm, A., Baker, I., & Frankenberg, C. (2015). Simulations of chlorophyll fluorescence incorporated into the community land model version 4. *Global Change Biology, 21*(9), 3469–3477.

Letelier, R. M., & Abbott, M. R. (1996). An analysis of chlorophyll fluorescence algorithms for the moderate resolution imaging spectrometer (modis). *Remote Sensing of Environment, 58*(2), 215–223.

Lichtenthaler, H. K., & Rinderle, U. (1988). The role of chlorophyll fluorescence in the detection of stress conditions in plants. *CRC Critical Reviews in Analytical Chemistry, 19*(sup1), S29–S85.

Lichtenthaler, H. K., Buschmann, C., Rinderle, U., & Schmuck, G. (1986). Application of chlorophyll fluorescence in ecophysiology. *Radiation and Environmental Biophysics, 25*(4), 297–308.

Luus, K. A., Commane, R., Parazoo, N. C., Benmergui, J., Euskirchen, E. S., Frankenberg, C., Joiner, J., Lindaas, J., Miller, C. E., Oechel, W. C., Zona, D., Wofsy, S., & Lin, J. C. (2017). Tundra photosynthesis captured by satellite-observed solar-induced chlorophyll fluorescence. *Geophysical Research Letters*. http://dx.doi.org/10.1002/2016GL070842.

Maxwell, K., & Johnson, G. N. (2000). Chlorophyll fluorescenceâĂŤa practical guide. *Journal of Experimental Botany, 51*(345), 659–668.

Meroni, M., Rossini, M., Guanter, L., Alonso, L., Rascher, U., Colombo, R., & Moreno, J. (2009). Remote sensing of solar-induced chlorophyll fluorescence: Review of methods and applications. *Remote Sensing of Environment, 113*(10), 2037–2051. http://dx.doi.org/10.1016/j.rse.2009.05.003.

Migliavacca, M., Perez-Priego, O., Rossini, M., El-Madany, T. S., Moreno, G., Tol, C.v.d., Rascher, U., Berninger, A., Bessenbacher, V., Burkart, A., et al. (2017). Plant functional traits and canopy structure control the relationship between photosynthetic CO_2 uptake and far-red sun-induced fluorescence in a mediterranean grassland under different nutrient availability. *New Phytologist, 214*, 1078–1091.

Moreno, J., Alonso, L., Delegido, J., Rivera, J. P., Ruiz-Verdú, A., Sabater, N., Tenjo, C., Verrelst, J., & Vicent, J. (2014). Flex (fluorescence explorer) mission: Observation fluorescence as a new remote sensing technique to study the global terrestrial vegetation state. *Revista de Teledetección, 41*, 111–119.

Moya, I., Camenen, L., Evain, S., Goulas, Y., Cerovic, Z. G., Latouche, G., Flexas, J., & Ounis, A. (2004). A new instrument for passive remote sensing 1. measurements of sunlight-induced chlorophyll fluorescence. *Remote Sensing of Environment, 91*(2), 186–197. http://dx.doi.org/10.1016/j.rse.2004.02.012.

Müller, N. J. C. (1874). Untersuchungen über die diffusion der atmosphärischen gase und die gasausscheidung unter verschiedenen beleuchtungs-bedingungen. *Jahrbucher fur Wissenschaftliche Botanik, 9*, 36–49.

Niyogi, K. K., & Truong, T. B. (2013). Evolution of flexible non-photochemical quenching mechanisms that regulate light harvesting in oxygenic photosynthesis. *Current Opinion in Plant Biology, 16*(3), 307–314.

O'Brien, D. M., Polonsky, I., O'Dell, C., & Carheden, A. (2009). *Algorithm theoretical basis document: The OCO simulator, Technical Report*. Fort Collins, CO: Cooperative Institute for Research in the Atmosphere, Colorado State University. ISSN 0737-5352-85. Technical report, ftp://ftp.cira.colostate.edu/ftp/TTaylor/publications/20090813_OCO_simulator.pdf.

O'Dell, C., Connor, B., Bösch, H., O'Brien, D., Frankenberg, C., Castano, R., Christi, M., Crisp, D., Eldering, A., Fisher, B., Gunson, M., McDuffie, J., Miller, C., Natraj, V., Oyafuso, F., Polonsky, I., Smyth, M., Taylor, T., Toon, G., Wennberg, P., & Wunch, D. (2011). The acos CO_2 retrieval algorithm—part 1: Description and validation against synthetic observations. *Atmospheric Measurement Techniques Discussions, 4*(5), 6097–6158.

Papageorgiou, G. C., et al. (2007). Chlorophyll a fluorescence: A signature of photosynthesis. In *19*. New York: Springer.

Parazoo, N. C., Barnes, E., Worden, J., Harper, A. B., Bowman, K. B., Frankenberg, C., Wolf, S., Litvak, M., & Keenan, T. F. (2015). Influence of enso and the nao on terrestrial carbon uptake in the texas-northern mexico region. *Global Biogeochemical Cycles, 29*(8), 1247–1265.

Park, Y.-I., Soon Chow, W., & Anderson, J. M. (1995). Light inactivation of functional photosystem ii in leaves of peas grown in moderate light depends on photon exposure. *Planta, 196*(3), 401–411.

Pfeilsticker, K., Erie, F., Funk, O., Veitel, H., & Platt, U. (1998). First geometrical pathlengths probability density function derivation of the skylight from spectroscopically highly resolving oxygen A-band observations 1. Measurement technique, atmospheric observations and model calculations. *Journal of Geophysical Research, 103*(D10), 11483.

Plascyk, J. A., & Gabriel, F. C. (Jan 1975). The Fraunhofer line discriminator MKII-an airborne instrument for precise and standardized ecological luminescence measurement. *IEEE Transactions on Instrumentation and Measurement, 24*(4), 306–313.

Platt, U., & Stutz, J. (2008). Differential absorption spectroscopy. New York: Springer.

Porcar-Castell, A., TyystjÃd'rvi, E., Atherton, J., Tol, C. V. D., Flexas, J., PfÄijndel, E. E., Moreno, J., Frankenberg, C., & Berry, J. A. (2014). Linking chlorophyll a fluorescence to photosynthesis for remote sensing applications: Mechanisms and challenges. *Journal of Experimental Botany, 65*(15), 4065. http://dx.doi.org/10.1093/jxb/eru191.

Potter, A. E., Mendell, W., & Morgan, T. (1984). Lunar luminescence and the filling-in of fraunhofer lines in moonlight. *Journal of Geophysical Research Section C, 89*, C240.

Rascher, U., Gioli, B., & Miglietta, F. (2008). FlexâĂŤfluorescence explorer: A remote sensing approach to quantify spatio-temporal variations of photosynthetic efficiency from space. In *Photosynthesis. Energy from the Sun* (pp. 1387–1390). Dordrecht: Springer.

Rascher, U., Agati, G., Alonso, L., Cecchi, G., Champagne, S., Colombo, R., Damm, A., Daumard, F., de Miguel, E., Fernandez, G., Franch, B., Franke, J., Gerbig, C., Gioli, B., Gomez, J. A., Goulas, Y., Guanter, L., Gutierrez de-la Camara, O., Hamdi, K., Hostert, P., Jimenez, M., Kosvancova, M., Lognoli, D., Meroni, M., Miglietta, F., Moersch, A., Moya, A., Neininger, B., Okujeni, A., Ounis, A., Palombi, L., Raimondi, V., Schickling, A., Sobrino, J. A., Stellmes, M., Toci, G., Toscano, P., Udelhoven, T., van der Linden, S., & Zaldei, A. (2009). CEFLES2: The remote sensing component to quantify photosynthetic efficiency from the leaf to the region by measuring sun-induced fluorescence in the oxygen absorption bands. *Biogeosciences, 6*(7), 1181–1198.

Rascher, U., Alonso, L., Burkart, A., Cilia, C., Cogliati, S., Colombo, R., Damm, A., Drusch, M., Guanter, L., Hanus, J., et al. (2015). Sun-induced fluorescence–a new probe of photosynthesis: First maps from the imaging spectrometer hyplant. *Global Change Biology, 21*(12), 4673–4684.

Rossini, M., Nedbal, L., Guanter, L., Ač, A., Alonso, L., Burkart, A., Cogliati, S., Colombo, R., Damm, A., Drusch, M., Hanus, J., Janoutova, R., Julitta, T., Kokkalis, P., Moreno, J., Novotny, J., Panigada, C., Pinto, F., Schickling, A., SchÃijttemeyer, D., Zemek, F., & Rascher, U. (2015). Red and far red sun-induced chlorophyll fluorescence as a measure of plant photosynthesis. *Geophysical Research Letters, 42*(6), 1632–1639. http://dx.doi.org/10.1002/2014GL062943.

Rossini, M., Meroni, M., Celesti, M., Cogliati, S., Julitta, T., Panigada, C., Rascher, U., Tol, C.v.d., & Colombo, R. (2016). Analysis of red and far-red sun-induced chlorophyll fluorescence and their ratio in different canopies based on observed and modeled data. *Remote Sensing, 8*(5), 412.

Sanders, A. F. J., Verstraeten, W. W., Kooreman, M. L., van Leth, T. C., Beringer, J., & Joiner, J. (2016). Space-borne sun-induced vegetation fluorescence time series from 2007 to 2015 evaluated with australian flux tower measurements. *Remote Sensing, 8*(11), 895.

Sanghavi, S., Martonchik, J. V., Landgraf, J., & Platt, U. (2012). Retrieval of the optical depth and vertical distribution of particulate scatterers in the atmosphere using O_2 a-and b-band sciamachy observations over Kanpur: A case study. *Atmospheric Measurement Techniques, 5*(5), 1099.

Schäfer, C., & Björkman, O. (1989). Relationship between efficiency of photosynthetic energy conversion and chlorophyll fluorescence quenching in upland cotton (*Gssypium hirsutum* L.). *Planta, 178*(3), 367–376.

Schlau-Cohen, G. S. (2015). Principles of light harvesting from single photosynthetic complexes. *Interface Focus, 5*(3), 2015. http://dx.doi.org/10.1098/rsfs.2014.0088.

Schreiber, U., Schliwa, U., & Bilger, W. (1986). Continuous recording of photochemical and non-photochemical chlorophyll fluorescence quenching with a new type of modulation fluorometer. *Photosynthesis Research, 10*(1–2), 51–62.

Stoll, M., Smorenburg, K., Visser, H., Crocco, L., Heilimo, J., Honig, A., et al. (1999). Flex: Fluorescence explorer. In *Remote sensing* (pp. 487–494). Bellingham: International Society for Optics and Photonics.

Sun, Y., Fu, R., Dickinson, R., Joiner, J., Frankenberg, C., Gu, L., Xia, Y., & Fernando, N. (2015). Drought onset mechanisms revealed by satellite solar-induced chlorophyll fluorescence: Insights from two contrasting extreme events. *Journal of Geophysical Research, Biogeosciences, 120*(11), 2427–2440.

Thuillier, G., Floyd, L., Woods, T. N., Cebula, R., Hilsenrath, E., Hersé, M., & Labs, D. (2004). Solar irradiance reference spectra for two solar active levels. *Advances in Space Research, 34*(2), 256–261.

Tol, C., Verhoef, W., Timmermans, J., Verhoef, A., & Su, Z. (2009). An integrated model of soil-canopy spectral radiances, photosynthesis, fluorescence, temperature and energy balance. *Biogeosciences, 6*(12), 3109–3129.

Tol, C., Berry, J. A., Campbell, P. K. E., & Rascher, U. (2014). Models of fluorescence and photosynthesis for interpreting measurements of solar-induced chlorophyll fluorescence. *Journal of Geophysical Research, Biogeosciences, 119*(12), 2312–2327.

Tol, C.v.d., Rossini, M., Cogliati, S., Verhoef, W., Colombo, R., Rascher, U., & Mohammed, G. (December 2016). A model and measurement comparison of diurnal cycles of suninduced chlorophyll fluorescence of crops. *Remote Sensing of Environment, 186*(C), 663–677.

Vasilkov, A., Joiner, J., & Spurr, R. (2013). Note on rotational-raman scattering in the O_2 a- and b-bands. *Atmospheric Measurement Techniques, 6*(4), 981–990. http://dx.doi.org/10.5194/amt-6-981-2013.

Verrelst, J., Pablo Rivera, J., Tol, C.v.d., Magnani, F., Mohammed, G., & Moreno, J. (2015). Global sensitivity analysis of the scope model: What drives simulated canopy-leaving sun-induced fluorescence? *Remote Sensing of Environment, 166*, 8–21.

Verrelst, J., Tol, C.v.d., Magnani, F., Sabater, N., Pablo Rivera, J., Mohammed, G., & Moreno, J. (2016). Evaluating the predictive power of sun-induced chlorophyll fluorescence to estimate net photosynthesis of vegetation canopies: A scope modeling study. *Remote Sensing of Environment, 176*, 139–151.

Vilfan, N., Tol, C. V. D., Muller, O., Rascher, U., & Verhoef, W. (2016). Fluspect-b: A model for leaf fluorescence, reflectance and transmittancespectra. *Remote Sensing of Environment, 186*, 596–615. http://dx.doi.org/10.1016/j.rse.2016.09.017.

Wieneke, S., Ahrends, H., Damm, A., Pinto, F., Stadler, A., Rossini, M., & Rascher, U. (2016). Airborne based spectroscopy of red and farred sun-induced chlorophyll fluorescence: Implications for improved estimates of gross primary productivity. *Remote Sensing of Environment, 184*, 654–667. http://dx.doi.org/10.1016/j.rse.2016.07.025.

Wolanin, A., Rozanov, V. V., Dinter, T., NoÃńl, S., Vountas, M., Burrows, J. P., & Bracher, A. (2015). Global retrieval of marine and terrestrial chlorophyll fluorescence at its red peak using hyperspectral top of atmosphere radiance measurements: Feasibility study and first results. *Remote Sensing of Environment, 166*, 243–261. http://dx.doi.org/10.1016/j.rse.2015.05.018. ISSN 0034–4257.

Woodrow, I. E., & Berry, J. A. (1988). Enzymatic regulation of photosynthetic CO_2, fixation in c3 plants. *Annual Review of Plant Physiology and Plant Molecular Biology, 39*(1), 533–594.

Xing, X.-G., Zhao, D.-Z., Liu, Y.-G., Yang, J.-H., Xiu, P., & Lin, W. (2007). An overview of remote sensing of chlorophyll fluorescence. *Ocean Science Journal, 42*(1), 49–59.

Yang, X., Tang, J., Mustard, J. F., Lee, J.-E., Rossini, M., Joiner, J., William Munger, J., Kornfeld, A., & Richardson, A. D. (2015). Solar-induced chlorophyll fluorescence that correlates with canopy photosynthesis on diurnal and seasonal scales in a temperate deciduous forest. *Geophysical Research Letters, 42*(8), 2977–2987.

Yoshida, Y., Joiner, J., Tucker, C., Berry, J., Lee, J.-E., Walker, G., Reichle, R., Koster, R., Lyapustin, A., & Wang, Y. (2015). The 2010 russian drought impact on satellite measurements of solar-induced chlorophyll fluorescence: Insights from modeling and comparisons with parameters derived from satellite reflectances. *Remote Sensing of Environment, 166*, 163–177.

Zaks, J., Amarnath, K., Kramer, D. M., Niyogi, K. K., & Fleming, G. R. (2012). A kinetic model of rapidly reversible nonphotochemical quenching. *Proceedings of the National Academy of Sciences, 109*(39), 15757–15762.

Zarco-Tejada, P. J., Pushnik, J. C., Dobrowski, S., & Ustin, S. L. (Jan 2003). Steady-state chlorophyll a fluorescence detection from canopy derivative reflectance and double-peak red-edge effects. *Remote Sensing of Environment, 84*(2), 283–294.

Zhang, Q., Xiao, X., Braswell, B., Linder, E., Baret, F., & Moore, B. (2005). Estimating light absorption by chlorophyll, leaf and canopy in a deciduous broadleaf forest using modis data and a radiative transfer model. *Remote Sensing of Environment, 99*(3), 357–371.

Zhang, Y., Guanter, L., Berry, J. A., Joiner, J., Tol, C., Huete, A., Gitelson, A., Voigt, M., & Köhler, P. (2014). Estimation of vegetation photosynthetic capacity from space-based measurements of chlorophyll fluorescence for terrestrial biosphere models. *Global Change Biology, 20*(12), 3727–3742.

Zhang, Y., Guanter, L., Berry, J. A., Tol, C.v.d., Yang, X., Tang, J., & Zhang, F. (2016). Model-based analysis of the relationship between sun-induced chlorophyll fluorescence and gross primary production for remote sensing applications. *Remote Sensing of Environment, 187*, 145–155.